Article

# Discovery and Mechanism of SARS-CoV-2 Main Protease Inhibitors

Sarah Huff,[▽] Indrasena Reddy Kummetha,[▽] Shashi Kant Tiwari, Matthew B. Huante, Alex E. Clark, Shaobo Wang, William Bray, Davey Smith, Aaron F. Carlin, Mark Endsley, and Tariq M. Rana*
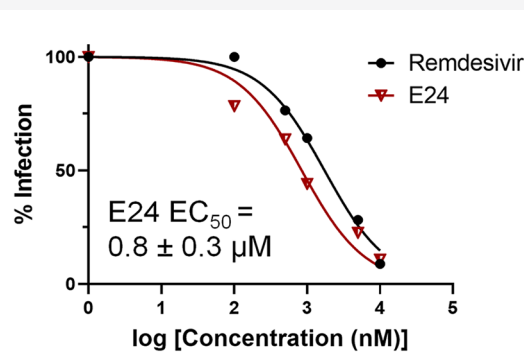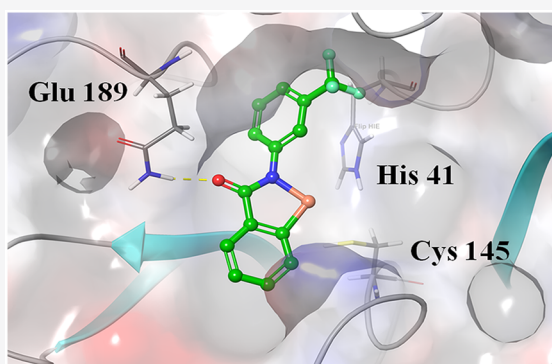
Read Online

ACCESS | 📊 Metrics & More | 📄 Article Recommendations | 🔘 Supporting Information

**ABSTRACT:** The emergence of a new coronavirus, severe acute respiratory syndrome coronavirus 2 (SARS-CoV-2), presents an urgent public health crisis. Without available targeted therapies, treatment options remain limited for COVID-19 patients. Using medicinal chemistry and rational drug design strategies, we identify a 2-phenyl-1,2-benzoselenazol-3-one class of compounds targeting the SARS-CoV-2 main protease ($M^{pro}$). FRET-based screening against recombinant SARS-CoV-2 $M^{pro}$ identified six compounds that inhibit proteolysis with nanomolar $IC_{50}$ values. Preincubation dilution experiments and molecular docking determined that the inhibition of SARS-CoV-2 $M^{pro}$ can occur by either covalent or noncovalent mechanisms, and lead E04 was determined to inhibit $M^{pro}$ competitively. Lead E24 inhibited viral replication with a nanomolar $EC_{50}$ value (844 nM) in SARS-CoV-2-infected Vero E6 cells and was further confirmed to impair SARS-CoV-2 replication in human lung epithelial cells and human-induced pluripotent stem cell-derived 3D lung organoids. Altogether, these studies provide a structural framework and mechanism of $M^{pro}$ inhibition that should facilitate the design of future COVID-19 treatments.

## INTRODUCTION

Emergent β-coronavirus severe acute respiratory syndrome coronavirus 2 (SARS-CoV-2) causes COVID-19, for which there is a great need for a new targeted treatment. SARS-CoV-2 produces a spike protein that binds to host cell receptor ACE2 for entry.[1,2] Upon entry, the positive genomic RNA of SARS-CoV-2 will attach directly to the host ribosome and translate two large polyproteins, which are then processed by proteolysis into components for packaging new virions. This proteolysis is controlled by two protease enzymes, the coronavirus main protease ($M^{pro}$) and the papain-like protease ($PL^{pro}$).[2−6] An RNA-dependent RNA polymerase (RdRp) is also required to replicate the RNA genome.[2,7] As all four of these proteins are essential for viral replication, they are considered attractive drug targets for treating coronaviruses. Of these, $M^{pro}$ has been widely called the virus' "Achilles Heel" and is considered one of the most attractive targets for drug development against SARS-CoV-2. The main protease is an established drug target for similar (+)-ssRNA viruses such as HIV and hepatitis C,[8−14] although to date there are no approved therapies targeting SARS-CoV-2's main protease.

Some early studies have identified crystal structures of potential small-molecule binders of SARS-CoV-2 $M^{pro}$, which are predominately peptide-based scaffolds.[15−20] Jin et al. determined the first crystal structure of $M^{pro}$ in complex with the peptide inhibitor N3.[15] Additional crystal structures of two rationally designed covalent peptide inhibitors, **11a** and **11b**, were reported shortly thereafter by Dai et al.[16] Two additional reports demonstrated that the feline coronavirus drug GC376 also inhibits $M^{pro}$ and prevents viral replication in infected Vero cells.[17,20] Like **11a** and **11b**, GC376 is a peptide inhibitor that covalently modifies active site Cys 145. Several non-peptide small molecules have also been shown to inhibit $M^{pro}$ proteolysis in vitro, including the organoselenium compound ebselen; however, to date there is only limited knowledge of
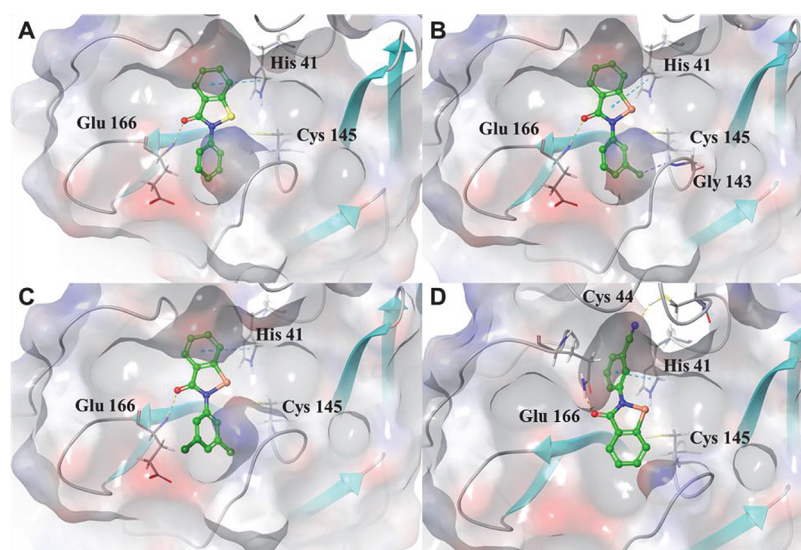
**Figure 1.** Docking poses of ebselen and 2-phenyl-1,2-benzoselenazol-3-one analogues. (A) Docking pose of ebselen bound to the catalytic site of SARS-CoV-2 $M^{pro}$. A hydrogen bond is present between the carbonyl oxygen atom of E01 and Glu 166. The benzoisoselenazole ring forms $\pi-\pi$ stacking interactions with catalytic His 41. (B) Docking pose of E19 bound to the catalytic site of SARS-CoV-2 $M^{pro}$. A hydrogen bond is present between the carbonyl oxygen atom of E19 and Glu 166. The benzoisoselenazole ring forms $\pi-\pi$ stacking interactions with catalytic His 41. The chlorine atom of E19 forms a halogen bond interaction with Gly 143. (C) Docking pose of E20 bound to the catalytic site of SARS-CoV-2 $M^{pro}$. $\pi-\pi$ stacking interactions are present between the benzoisoselenazole ring of E20 and catalytic His 41. A hydrogen bond is present between the carbonyl oxygen atom of E20 and Glu 166. (D) Docking pose of E25 bound to the catalytic site of SARS-CoV-2 $M^{pro}$. A hydrogen bond is present between the carbonyl oxygen atom of E25 and Glu 166. $\pi-\pi$ stacking interactions are present between the benzoisoselenazole ring of E25 and catalytic His 41. The nitrile group was observed to accept a hydrogen bond from Cys 44.

their mechanism of action and the cell-based evaluation of small molecules.[15,19] At this time, most studies targeting $M^{pro}$ are focused on screening existing compounds, and there has been little interest in further developing early hits using medicinal chemistry and rational drug design approaches. In this study, we sought to determine if such approaches could be applied to address the following questions: (1) can rational drug design and medicinal chemistry be used to improve the potencies of identified $M^{pro}$ inhibitors? (2) Can an enzymatic mechanism of inhibition be established for rationally designed $M^{pro}$ inhibitors? (3) Can rationally designed compounds inhibit viral replication *in vitro*? Finally, (4) how do rationally designed $M^{pro}$ inhibitors compare to existing treatments such as remdesivir?

To address these questions, we used the structure of the organoselenium compound ebselen as the basis for the rational design of improved $M^{pro}$ inhibitors. *In silico* docking at the SARS-CoV-2 $M^{pro}$ active site identified a class of 2-phenyl-1,2-benzoselenazol-3-one inhibitors with nanomolar proteolytic activities against recombinant SARS-CoV-2 $M^{pro}$ and improved physicochemical properties relative to those of their parent compound ebselen. Steady-state enzyme kinetics was used to determine that ebselen and its analogue E04 are competitive inhibitors of $M^{pro}$, and 2-phenyl-1,2-benzoselenazol-3-one inhibitors may follow either a noncovalent or reversible covalent mechanism. These compounds were also determined to show potent antiviral effects in multiple SARS-CoV-2-infected cell lines, with leads E24 and E25 reporting inhibitory activities comparable or better to that of the clinical antiviral treatment remdesivir ($EC_{50}$(E24) = 0.8 ± 0.3 $\mu$M, $EC_{50}$(E25) = 2.0 ± 1.1 $\mu$M, and $EC_{50}$(remdesivir) = 1.8 ± 1.3 $\mu$M). Furthermore, E24 was found to reduce viral replication in both Calu-3 human lung epithelial cells ($EC_{50}$(E24) = 1.3 ± 0.8

$\mu$M) and human iPSC-derived lung organoids infected with SARS-CoV-2.

## ■ RESULTS

**Identification of the 2-Phenyl-1,2-benzoselenazol-3-one Class of SARS-CoV-2 $M^{pro}$ Inhibitors.** Recently, a study showed that the organoselenium compound ebselen was able to bind SARS-CoV-2 $M^{pro}$ and inhibit proteolytic activity.[15] While it was determined that ebselen could partially covalently modify $M^{pro}$, the binding site was not identified. Using this information as a starting point, we sought to model ebselen in the active site of $M^{pro}$ to determine if organoselenium compounds could be rationally designed to target the catalytic site. Docking was performed in the Schrödinger software suite.[21−23] A crystal structure of the SARS-CoV-2 $M^{pro}$ bound to N3 (PDB ID 6UL7) was used to generate the docking grid as a 15 Å cube centered on the ligand N3. As observed in Figure 1A, the active site of $M^{pro}$ is expected to accommodate ebselen. Ebselen is predicted to bind in close proximity to catalytic His 41 and Cys 145, with the benzoisoselenazole ring forming $\pi-\pi$ stacking interactions with catalytic His 41. Binding is further stabilized by a hydrogen bond between the carbonyl oxygen atom of ebselen and Glu 166. These results are consistent with a recently reported crystal structure of SARS-CoV-2 $M^{pro}$ in complex with ebselen, which indicates that it primarily binds to the catalytic site of the enzyme and forms a selenyl sulfide bond with Cys 145; this was further confirmed by LC/MRM-MS.[24]

A series of 2-phenyl-1,2-benzoselenazol-3-one analogues was designed with substitutions primarily focused on the N-phenyl moiety. Substitutions included halogens (F, Cl, and Br) and hydrophobic groups ($CH_3$, $CF_3$, $SCH_3$, $OCH_3$, and $CH_2CH_3$) as well as several lipophilic replacements of the phenyl moiety. Potential inhibitors were docked and ranked by their docking

**Scheme 1. Synthesis of Ebselen Analogues**



Reagents and conditions: a). TEA, DCM, RT, 3h, b). tBuONa, Se powder, 130 °C, 12h.
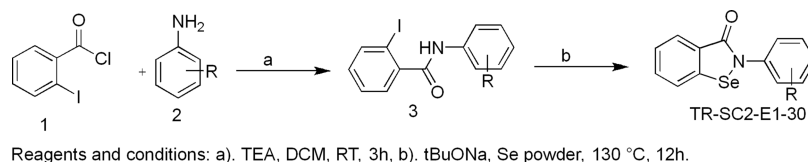
score. The docking poses of prospective analogues were evaluated for interactions with catalytic residues His 41 and Cys 145; compounds that were expected to form strong hydrogen bonds or $\pi$-interactions with these residues were prioritized for synthesis. Docking poses for ebselen and three of its analogues can be found in Figure 1. As observed in Figure 1 B, E19 is able to maintain the interactions with Glu 166 and catalytic His 41 that were observed for ebselen, while the *p*-chloro substituent group forms an additional halogen bond with the amide backbone of Gly 143. Similarly, the *m*-cyano group of E25 is able to accept a hydrogen bond from Cys 44 while maintaining the interactions of the parent compound with His 41 and Glu 166 (Figure 1 A and D). In Figure 1 C, E20 is expected to maintain the core interactions of the parent structure with His 41 and Glu 166, while *m,m*-dichloro substitutions occupy a larger region of the binding pocket to increase the entropy of the binding interaction. Docking poses for select additional compounds may be found in the Supporting Information (Figure S1).
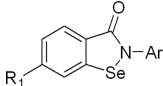
A total of 30 2-phenyl-1,2-benzoselenazol-3-one compounds were selected for synthesis according to Scheme 1 (Figure 1 E). Analogues were synthesized from commercially available acid chlorides and anilines in two steps. Nucleophilic acyl substitution in the presence of triethylamine yielded intermediate **3**. Ring closure to form the benzoisoselenazole ring proceeded in the presence of NaSeOtBu with selenium powder and sodium *tert*-butoxide in DMF to produce the final product. In total, 30 compounds were prepared according to this scheme, purified by column chromatography (hexane/ethyl acetate 70:30), and characterized by NMR and HRMS prior to the biological evaluation.

**The 2-Phenyl-1,2-benzoselenazol-3-one Class of Compounds Are Potent Inhibitors of Recombinant M^pro.** To determine if the 2-phenyl-1,2-benzoselenazol-3-one class of rationally designed compounds was also able to inhibit protease activity of SARS-CoV-2 M^pro, a FRET assay adapted from Muramatsu et al.[25] was used to assess the inhibitory potency of the compounds against SARS-CoV-2 M^pro at 10 $\mu$M. Ebselen was included as a positive control.[15] Of the 30 analogues tested, 22 inhibited M^pro proteolytic activity by >50%, while eight compounds showed no inhibition at this concentration. Full dose−response curves were generated for compounds showing >50% inhibition at 10 $\mu$M (Table 1). The $IC_{50}$ of ebselen was observed to be 0.33 $\mu$M, which was similar to the previously reported value of 0.67 $\mu$M.[15] Most 2-phenyl-1,2-benzoselenazol-3-one analogues reported $IC_{50}$ values between 1 and 7.4 $\mu$M. Compounds E04, E07, E19, E20, and E25 reported submicromolar $IC_{50}$ valuess ranging from 0.38 to 0.90 $\mu$M (Table 1). Additional reports have identified two peptide inhibitors, **11a** and **11b**, that were designed to inhibit the main protease with more potent $IC_{50}$ values (0.053 and 0.040 $\mu$M, respectively);[16] however, the observed $IC_{50}$ valuess for compounds E04, E07, E19, E20, and E25 are similar in range to that reported for the feline coronavirus drug GC376 (0.19 ± 0.04 $\mu$M).[17] In general, *meta*-substitution of

the *N*-phenyl moiety was favorable. Two of the most potent compounds, E19 and E20, featured a *meta*-substituted chlorobenzene, and the most potent analogue, E25, featured a *meta*-cyano group. As observed in Figure 1 B, the *p*-chloro substitution of E19 is positioned such that it can form a halogen bond with the amide backbone of Gly 143, while the 1,2-benzisoselenazole ring forms $\pi-\pi$ interactions with catalytic His 41 and a hydrogen bond to Glu 166. In Figure 1 D, the *m*-cyano group of E25 is able to accept a hydrogen bond from Cys 44 while maintaining the core interactions with the 1,2-benzisoselenazole ring, $\pi-\pi$ interactions with catalytic His 41, and a hydrogen bond to Glu 166. In both these examples, *meta*-substitution could enable additional favorable interactions with the binding site that are not supported by *ortho*- or *para*-substitution. In general, *para*-substitution of the *N*-phenyl ring was tolerated, with most $IC_{50}$ values in the micromolar range, while *ortho*-substitution was generally unfavorable. Compound E15 featured the only variation to the 1,2-benzisoselenazole ring, a methoxy group at the C6 position. As observed in Figure 1 A, the 1,2-benzisoselenazole ring of ebselen is expected to form $\pi-\pi$ interactions with catalytic His 41 and a hydrogen bond to Glu 166, with the C6 position oriented toward His 41. The addition of the methoxy group at this position is likely to impair the $\pi-\pi$ interactions expected with catalytic His 41 and could reposition the compound within the binding site such that the hydrogen bond to Glu 166 is weaker. This substitution was observed to reduce the potency against SARS-CoV-2 M^pro by ~20× relative to that of ebselen.

**2-Phenyl-1,2-benzoselenazol-3-one Inhibitors Can Inhibit M^pro Covalently or Noncovalently.** The selenium atom of ebselen is capable of forming a selenylsulfide bond (−Se−S−);[26−29] in Singh et al., the substitution of the Se atom with S or the mutation of the target active site Cys was observed to decrease inhibition.[29] In most cases, proteins covalently modified by ebselen may be rescued by the sulfhydryl reducing agents glutathione (GSH) and dithiothreitol (DTT). Previously, Jin et al. reported that ebselen was able to partially modify M^pro Cys residues and concluded that ebselen could inhibit M^pro by both covalent and noncovalent mechanisms.[15] To determine if 2-phenyl-1,2-benzoselenazol-3-one analogs were also able to covalently modify the active site of SARS-CoV-2 M^pro, we performed a preincubation dilution experiment where SARS-CoV-2 M^pro was incubated with 10 $\mu$M inhibitor for 30 min prior to 10× dilution with the reaction buffer. Upon dilution, rapidly reversible inhibitors dissociate from the enzyme active site, and the resulting activity is proportional to that observed for the final inhibitor concentration, in this case 1 $\mu$M. If the inhibitor dissociation is slow, then the enzyme−inhibitor complexes formed at high concentrations will persist after dilution and the resulting activity will instead be proportional to the initial concentration of 10 $\mu$M. The concentration range of 10 and 1 $\mu$M was selected as all compounds tested in this experiment showed full enzymatic inhibition at 10 $\mu$M and some activity at 1 $\mu$M,

**Table 1. Structures, Docking Scores, and *In Vitro* Data Summary of 2-Phenyl-1,2-benzoselenazol-3-one Analogues**

| Structure R1 | Structure Ar | Name | Enzymatic IC$_{50}$ (μM) | Antiviral EC$_{50}$ (μM) | Structure R1 | Structure Ar | Name | Enzymatic IC$_{50}$ (μM) | Antiviral EC$_{50}$ (μM) |
|---|---|---|---|---|---|---|---|---|---|
| H | phenyl | E01 | 0.33 ± 0.03 | >20 | H | 2-methoxy-5-fluorophenyl | E16 | 3.30 ± 0.74 | >20 |
| H | 4-fluorophenyl | E02 | 2.78 ± 1.0 | 16.7 ± 4.8 | H | 2-methoxy-4-fluorophenyl | E17 | 1.80 ± 0.88 | >20 |
| H | 2-(methylthio)phenyl | E03 | >10 | >20 | H | 4-ethylphenyl | E18 | 6.18 ± 1.74 | 6.5 ± 2.0 |
| H | 4-CF$_3$ phenyl | E04 | 0.90 ± 0.17 | 11.2 ± 1.3 | H | 3-chlorophenyl | E19 | 0.68 ± 0.28 | 17.4 ± 3.5 |
| H | 3,4-dimethylphenyl | E05 | >10 | 12.2 ± 1.7 | H | 3,5-dichlorophenyl | E20 | 0.64 ± 0.10 | 18.2 ± 3.6 |
| H | 4-fluorobenzyl | E06 | 1.00 ± 0.29 | >20 | H | 4-bromophenyl | E21 | 2.77 ± 0.67 | 5.2 ± 1.8 |
| H | 2,4-dimethoxybenzyl | E07 | 0.61 ± 0.44 | 26.5 ± 1.2 | H | 4-methylphenyl | E22 | 2.29 ± 0.95 | 15.4 ± 1.5 |
| H | 2-fluorophenyl | E08 | >10 | >20 | H | 2-methylphenyl | E23 | 7.43 ± 0.77 | 20.7 ± 2.8 |
| H | 4-CF$_3$ benzyl | E09 | >10 | 11.2 ± 3.7 | H | 3-CF$_3$ phenyl | E24 | 2.77 ± 0.51 | 0.8 ± 0.3 |
| H | 2-CF$_3$-4-fluorophenyl | E10 | >10 | >20 | H | 3-cyanophenyl | E25 | 0.38 ± 0.08 | 2.0 ± 1.1 |
| H | 2,6-difluorophenyl | E11 | 2.09 ± 0.97 | >20 | H | 2-methoxyphenyl | E26 | >10 | 15.1 ± 3.1 |
| H | 4-methoxybenzyl | E12 | >10 | >20 | H | 4-methoxyphenyl | E27 | 1.25 ± 0.35 | 1.7 ± 2.7 |
| H | 2-(trifluoromethoxy)-4-chlorophenyl | E13 | >10 | >20 | H | 4-hexylphenyl | E28 | 5.56 ± 1.85 | 17.3 ± 3.7 |
| H | 2-methoxy-5-chlorophenyl | E14 | >10 | >20 | H | 4-hexylphenyl | E29 | 2.69 ± 0.24 | >20 |
| OCH$_3$ | phenyl | E15 | 6.40 ± 0.78 | 11.2 ± 1.3 | H | 4-butylphenyl | E30 | >10 | >20 |

typically between 15 and 50% wt activity. As previous reports have indicated that the covalent modification of Cys residues by ebselen is sensitive to reversal by reducing agents such as DTT or glutathione, we removed DTT from the assay buffer for these experiments.

The effect of dilution on the reaction rate of SARS-CoV-2 M$^{pro}$ preincubated with a 10 μM concentration of compounds E01 (ebselen), E04, E07, E19, E20, and E25 can be observed in Figure 2. The effect of the simultaneous addition of the substrate and either 1 or 10 μM inhibitor on the rate of SARS-
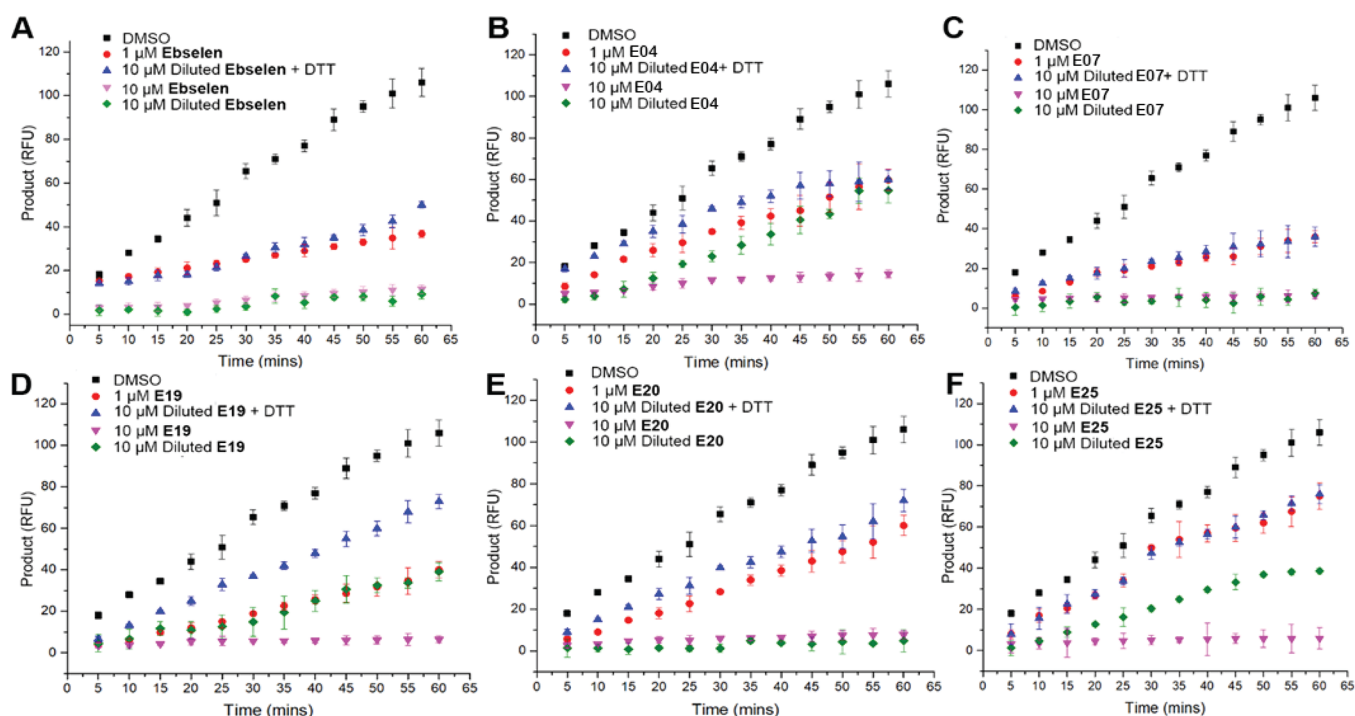
**Figure 2.** Ebselen and its analogues can covalently modify SARS-CoV-2 M$^{pro}$ in the absence of reducing agents. (A) Ebselen is a reversible covalent inhibitor of SARS-CoV-2 M$^{pro}$. The product formation over time was reduced by approximately 65% by 1 $\mu$M ebselen (red) and by 89% by 10 $\mu$M ebselen (purple) relative to that with the DMSO control (black) when added simultaneously with the fluorogenic substrate. Upon 10× dilution in an assay buffer without DTT, the product formation of SARS-CoV-2 M$^{pro}$ preincubated with 10 $\mu$M ebselen (green) was reduced by 91%, which is comparable to an undiluted concentration of 10 $\mu$M. When diluted in the presence of DTT, the product formation of SARS-CoV-2 M$^{pro}$ preincubated with 10 $\mu$M of ebselen (blue) was reduced by 53% relative to that with the DMSO control, similar to that observed for a final concentration of 1 $\mu$M. These data indicate that ebselen can covalently modify SARS-CoV-2 M$^{pro}$, although this modification is reversible in the presence of strong reducing agents. (B) Compound E04 is a rapidly reversible inhibitor of SARS-CoV-2 M$^{pro}$. Upon 10× dilution, the product formation of SARS-CoV-2 M$^{pro}$ preincubated with 10 $\mu$M E04 in the absence of DTT (green) was reduced by 48% relative to that with the DMSO control, similar to that observed for a final concentration of 1 $\mu$M E04 (44% inhibition), while the simultaneous addition of the substrate and 10 $\mu$M E04 reduced the product formation by 86%. Similar results were observed for SARS-CoV-2 M$^{pro}$ preincubated with 10 $\mu$M E04 in the presence of DTT (blue, 43% inhibition). (C) Compound E07 is a reversible covalent inhibitor of SARS-CoV-2 M$^{pro}$. (D) Compound E19 is a rapidly reversible inhibitor of SARS-CoV-2 M$^{pro}$. (E) Compound E20 is a reversible covalent inhibitor of SARS-CoV-2 M$^{pro}$. (F) Compound E25 is a reversible covalent inhibitor of SARS-CoV-2 M$^{pro}$. Upon 10× dilution, the product formation of SARS-CoV-2 M$^{pro}$ preincubated with 10 $\mu$M E25 in the absence of DTT (green) was reduced by 64% relative to that with the DMSO control. The simultaneous addition of the substrate and 10 $\mu$M 25 reduced product formation by 94%, while the simultaneous addition of the substrate and 1 $\mu$M E25 reduced product formation by 29%. These data suggest that while E25 may covalently modify SARS-CoV-2 M$^{pro}$, the formation of the covalent adduct was incomplete after 30 min of incubation.

CoV-2 M$^{pro}$ was included for each inhibitor as a comparison. As seen in Figure 2 A, C, and E, dilution of the protease-inhibitor reaction mixture did not alter the reaction rate when M$^{pro}$ was incubated with ebselen, E07, or E20, indicating that these compounds likely inhibit M$^{pro}$ by covalent modification. However, the dilution of M$^{pro}$ treated with compounds E04 and E19 did result in a reaction rate similar to that observed for a 1 $\mu$M concentration of the undiluted compound, indicating that these analogues are rapidly reversible inhibitors of SARS-CoV-2 M$^{pro}$ (Figure 2 B and D). Interestingly, the dilution of the M$^{pro}$/E25 reaction mixture did show some recovery of the enzymatic activity but not a complete recovery comparable to the activity observed for M$^{pro}$ treated with 1 $\mu$M E25 without dilution (Figure 2 F). These results could suggest that the covalent modification of M$^{pro}$ was incomplete in the 30 min preincubation period. To determine if M$^{pro}$ inhibition by 2-phenyl-1,2-benzoselenazol-3-one analogues is sensitive to reducing agents, the experiment was repeated with the presence of 1 mM DTT in the assay buffer. Under these conditions, the dilution of the reaction mixtures was sufficient to recover the enzymatic activity, suggesting that any covalent

adduct formed with M$^{pro}$ Cys residues was reduced such that the enzyme—inhibitor complex dissociated. These results indicate that while ebselen and some 2-phenyl-1,2-benzoselenazol-3-one analogues are able to covalently modify active M$^{pro}$ Cys residues, this covalent modification is reversible in a reducing environment. It is also possible that 2-phenyl-1,2-benzoselenazol-3-one analogues can inhibit M$^{pro}$ noncovalently, as observed for compounds E04 and E20.

**2-Phenyl-1,2-benzoselenazol-3-one Inhibitor E04 and Ebselen Are Competitive Inhibitors of M$^{pro}$.** The mechanism of M$^{pro}$ inhibition by ebselen and E04 was further characterized by steady-state enzyme kinetics (Figure 3). The reaction rates of untreated (wild-type) M$^{pro}$ at varying substrate concentrations and M$^{pro}$ in the presence of 0.5, 1, 5, and 10 $\mu$M E01 and E04 were determined, and the data were globally fit to a generalized mixed-model equation as described in the Inhibition Mechanism section. In this mechanism, the binding of the inhibitor to the ES complex is described by $\alpha K_i$, where $K_i$ is the dissociation constant. An value of $\alpha \gg 1$ provided a better fit of the data for both inhibitors, suggesting a weak binding to the ES complex and a
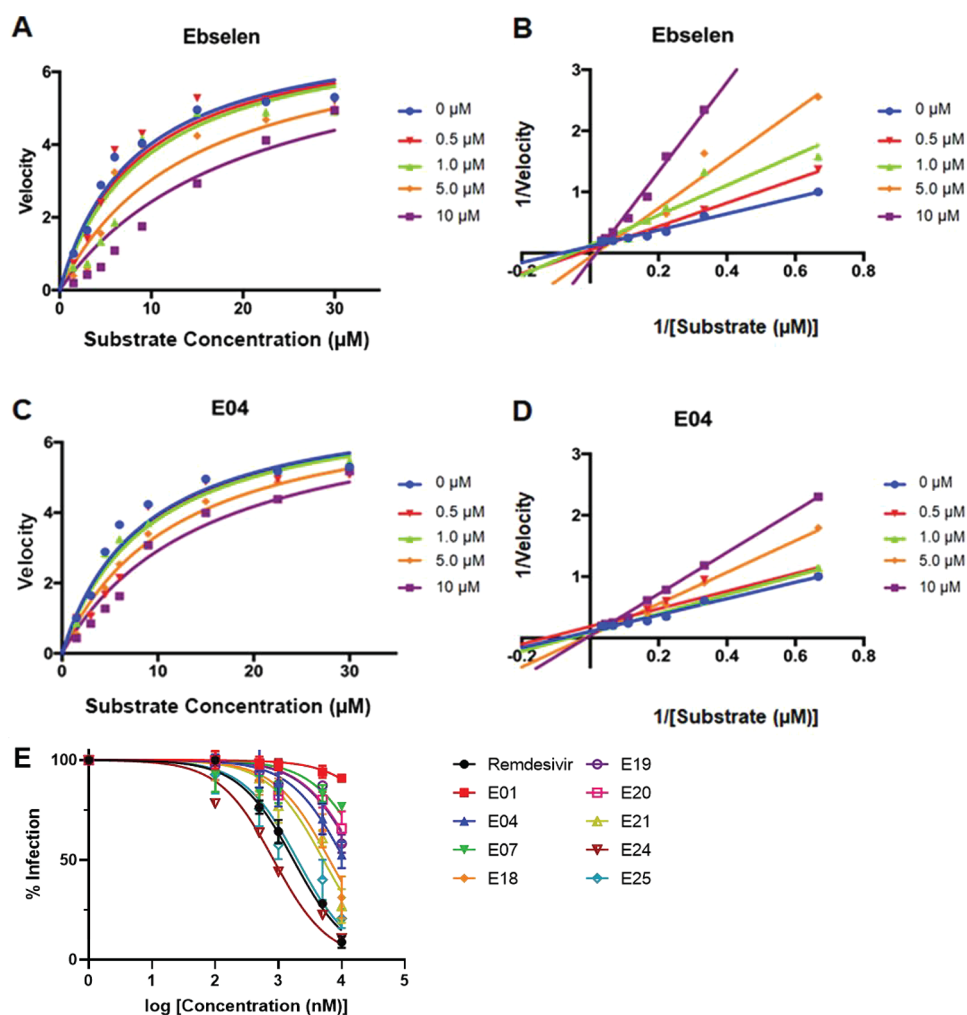
**Figure 3.** Ebselen and E04 are competitive inhibitors of the SARS-CoV-2 main protease. (A) $M^{pro}$ exposed to varying concentrations of ebselen reached a common $V_{max}$ at 30 $\mu$M substrate (B) All ebselen conditions converge on a common y-intercept, indicating that $V_{max}$ is independent of the inhibitor concentration, which is consistent with a competitive mechanism of inhibition. (C) $M^{pro}$ exposed to varying concentrations of E04 reached a common $V_{max}$ at 30 $\mu$M substrate (D) All E04 conditions converge on a common y-intercept, indicating that $V_{max}$ is independent of the inhibitor concentration, which is consistent with a competitive mechanism of inhibition. (E) Antiviral activity of select compounds. Vero E6 cells were pretreated with varying doses of the compound, then infected with SARS-CoV-2 to a multiplicity of infection (MOI) of 0.01. After 72 h, cell proliferation was determined. Remdesivir is included as a positive control ($EC_{50}$ = 1.8 $\pm$ 1.3 $\mu$M).

preference for the free enzyme. A plot of the reaction velocity versus the substrate concentration shows that when $M^{pro}$ is treated with either ebselen or E04, $V_{max}$ recovers to that observed for wild-type $M^{pro}$ at substrate concentrations of 30 $\mu$M (Figure 3 A and C). A double-reciprocal plot shows that for both compounds $K_m$ is dependent on [I] while $V_{max}$ remains consistent (Figure 3 B and D). These results indicate that ebselen and E04 are likely competitive inhibitors of $M^{pro}$.

**2-Phenyl-1,2-benzoselenazol-3-one Analogues Are Potent Antiviral Agents *In Vitro*.** To determine if 2-phenyl-1,2-benzoselenazol-3-oneanalogues were able to impair SARS-CoV-2 replication, the compounds were screened against infected Vero E6 cells at doses ranging from 20 to 0.1 $\mu$M to determine the cellular $EC_{50}$ value (Figures 3 E and S2 and Table 2). Briefly, cells were pretreated with compound for 1 h, then infected with SARS-CoV-2 (USA_WA01/2020) at a multiplicity of infection (MOI) of 0.01 for 1.5 h. Cells were washed, the compounds were reapplied, and cells were then incubated for 72 h prior to recording cthe ell proliferation. As a virus infection reduces cell proliferation

**Table 2. Antiviral Activity and logD Values of Select 2-Phenyl-1,2-benzoselenazol-3-one Analogues[a]**

| compound | antiviral $EC_{50}$ ($\mu$M) | logD pH 7.4 | compound | antiviral $EC_{50}$ ($\mu$M) | logD pH 7.4 |
|---|---|---|---|---|---|
| ebselen | >20 | 0.92 | remdesivir | 1.8 $\pm$ 1.2 | ND |
| E04 | 11.2 $\pm$ 1.3 | 3.19 | E20 | 18.2 $\pm$ 3.6 | 1.67 |
| E07 | 26.5 $\pm$ 1.2 | 0.85 | E21 | 5.2 $\pm$ 1.8 | 1.46 |
| E18 | 6.5 $\pm$ 2.0 | 2.87 | E24 | 0.8 $\pm$ 0.3 | 3.18 |
| E19 | 17.4 $\pm$ 3.5 | 1.53 | E25 | 2.0 $\pm$ 1.1 | 1.45 |

[a]ND, not determined.

and leads to cell death, only those compounds that show increased cell survival relative to that of the DMSO negative control are considered to have antiviral activity. In this way, compounds that are likely to be cytotoxic to Vero E6 cells at the concentrations tested are excluded as potential hits. Ebselen and remdesivir were included as positive controls. The antiviral activity of each compound is reported in Table 1. Most compounds reported $EC_{50}$ valuess in the micromolar range, and compounds E18, E21, and E25 showed antiviral

potencies similar to that of remdesivir (Tables 1 and 2 and Figure 3 E). The most potent compound, E24, showed a nanomolar antiviral potency (EC$_{50}$ = 0.84 ± 0.3 μM). This is within range of the most potent M$^{pro}$ inhibitors reported to date, including the rationally designed peptidyl inhibitors 11a and 11b (EC$_{50}$ = 0.53 ± 0.01 and 0.72 ± 0.09 μM, respectively)[16] and the feline coronavirus drug GC376 (EC$_{50}$ = 0.92 μM).[17] Interestingly, all three of these inhibitors are peptides that contain a similar warhead for the covalent modification of active site Cys 145. We demonstrated that the 2-phenyl-1,2-benzoselenazol-3-one class of inhibitors may inhibit M$^{pro}$ either covalently or noncovalently (Figure 2).

For some compounds, the potencies of the 2-phenyl-1,2-benzoselenazol-3-one analogues were reduced in the Vero cell assay relative to those in the FRET assay using recombinant M$^{pro}$. For example, while E04, E19, E20, and E25 reported nanomolar IC$_{50}$ valuess against recombinant M$^{pro}$ (IC$_{50}$ = 0.38−0.90 μM), their EC$_{50}$ valuess in the antiviral assay were in the micromolar range (2.0−18.2 μM). As these compounds are not expected to prevent viral entry into the cells, their antiviral potency will be a function of a variety of factors, including cell membrane permeability, efflux rate, and cellular metabolic pathways. The antiviral assays were also conducted over a 72 h incubation period, while the FRET assay was performed in a 1 h time frame, further complicating a direct comparison of potencies across these two assay systems. As observed in the preincubation dilution assays, many of the 2-phenyl-1,2-benzoselenazol-3-one analogues are sensitive to reducing agents, and their inhibitory potency could be affected by intracellular reducing mechanisms. While the exact potencies varied, in general compounds that were inactive against recombinant M$^{pro}$ were also inactive in the Vero E6 cell antiviral assays.

### 2-Phenyl-1,2-benzoselenazol-3-one Compounds Show Improved LogD Values Relative to Ebselen.

LogD values were also determined for ebselen and 2-phenyl-1,2-benzoselenazol-3-onecompounds E04, E07, E18, E19, E20, E21, E24, and E25 (Table 2). Meta-analyses of pharmaceutical drug development projects have identified the importance of logD in identifying compounds that are more likely to feature favorable clearance rates and membrane permeabilities; one such study found that compounds with a molecular weight of 350 g/mol and a logD of 1.5 had a 25% success rate of being advanced to clinical trials.[30−34] By analyzing the logD values for these analogues at this stage, we are able to predict which compounds are most likely to show favorable pharmacokinetic properties in future in vivo models. We may also determine if logD optimization can be useful in refining these compounds as antiviral agents prior to an in vivo study. As observed in Table 2, logD values are generally in the ideal range for most orally available drugs (Table 2, entries1−3).[30−33] Furthermore, logD values were broadly observed to correlate with the antiviral activity, where compounds with higher logD values (E18, and E24) showed greater antiviral potencies than those with low logD values (E07, E19, and E20). These data indicate that the logD value is a critical parameter for optimizing the antiviral potencies of these compounds.

### 2-Phenyl-1,2-benzoselenazol-3-one Analogues Show Antiviral Properties in Human Lung Cells.

To further confirm the antiviral properties observed in the Vero E6 cell assay, four compounds were selected foran additional evaluation in human lung epithelial cells. Ebselen and remdesivir were both included as positive controls. As before,

Calu-3 cells were pretreated with 0.1−20 μM concentrations of the compound for 1 h prior to infection with SARS-CoV-2 (USA_WA01/2020; MOI = 0.1) for 1.5 h. Cells were washed, the compounds were reapplied, and cells were then incubated for 24 h prior to the isolation and quantification of intracellular and supernatant viral RNA by RT-qPCR. Table 3 lists the antiviral EC$_{50}$ values of ebselen, remdesivir, E04, E18, E21, and E24 in Calu-3 cells.

**Table 3. Antiviral Activity of Select 2-Phenyl-1,2-benzoselenazol-3-one Analogues in Calu-3 Cells**

| compound | EC$_{50}$ (μM) | compound | EC$_{50}$ (μM) |
| --- | --- | --- | --- |
| ebselen | 5.0 ± 4.0 | remdesivir | 0.8 ± 0.6 |
| E04 | 2.8 ± 1.3 | E21 | 15.7 ± 4.3 |
| E18 | 8.8 ± 5.4 | E24 | 1.3 ± 0.8 |

In this model, remdesivir appears to be slightly more potent than in the Vero E6 cell proliferation assays (EC$_{50}$ = 0.8 ± 0.6 and 1.8 ± 1.2 μM, respectively); interestingly, this slight improvement in potency in human cell models was also observed for remdesivir by Dittmer et al.[35] and Jang et al.[36] in Calu-3 cells and by Choi et al.[37] in hESC- and hiPSC-derived cardiomyocytes. The difference in potency could be due to the variations in experimental conditions, including the cell lines and infection rates. Additionally, a recent comparison of commonly used cell models for SARS-CoV-2 antiviral assays by Dittmer et al. indicated that entry mechanisms vary for Calu-3 and Vero cells, where entry in Calu-3 cells was pH-independent and relied on transmembrane protease serine 2 (TMPRSS2) and entry to Vero cells was reliant upon acid-dependent endosomal proteases and low pH levels.[35] These variations in entry mechanisms resulted in significant alterations in the drug efficacy, particularly for compounds that targeted host proteases.[35] However, compounds that target the virus directly, like remdesivir, should remain active across cell types. As our 2-phenyl-1,2-benzoselenazol-3-one analogues target the SARS-CoV-2 main protease, we expected to retain antiviral activity for these compounds as well.

In Calu-3, ebselen had an EC$_{50}$ of 5.0 μM, which is in the range of reported EC$_{50}$ values observed by Vero E6 cell proliferation assays.[24] Of the remaining 2-phenyl-1,2-benzoselenazol-3-one analogues, E18 and E24 had EC$_{50}$ values consistent with those observed in Vero E6 cells (E18 EC$_{50}$ = 8.8 ± 5.4 μM; E24 EC$_{50}$ = 1.3 ± 0.8 μM). E04 showed a marked improvement in potency, with a fourfold reduction in EC$_{50}$ in Calu-3 cells (2.8 ± 1.3 μM) versus that in Vero E6 (11.2 ± 1.3 μM). E21, however, showed a threefold reduction in potency Calu-3 cells (EC$_{50}$ = 15.7 ± 4.3 μM) relative to that in Vero E6 (EC$_{50}$ = 5.2 ± 1.8 μM). This difference in potency observed for E04 and E21 could be due to changes in either the compound permeability or stability in various cells and culture conditions. Importantly, all compounds remained active antivirals in human lung epithelial cells, indicating that the antiviral properties of the analogues are robust across assay systems and relevant to human models.

### Compound E24 Reduces SARS-CoV-2 Viral Infection in Human Lung Organoids.

The most potent compound from our antiviral screens, E24, was evaluated in a lung organoid model derived from human-induced pluripotent stem cells (iPSC). Human iPSC-derived lung 3D organoids were generated as described by Tiwari et al.[38] Organoids were characterized as containing epithelial cells, alveolar types 1 and
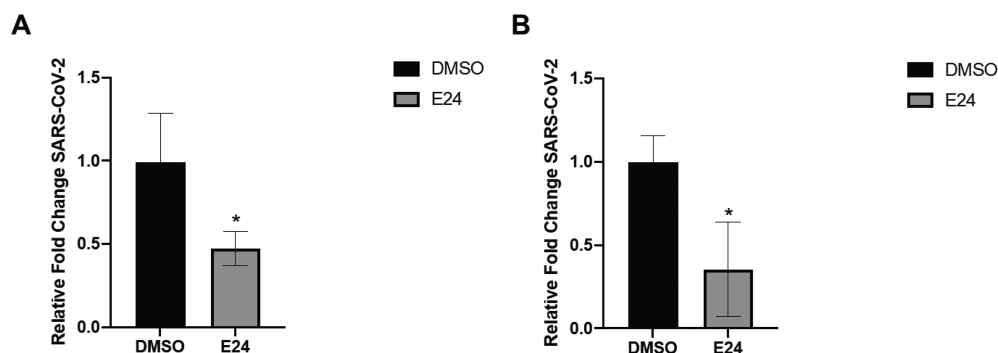
**Figure 4.** E24 inhibits SARS-CoV-2 replication in infected human iPSC-derived lung organoids. Sixty-day-old lung organoids were infected with the SARS-CoV-2 USA-WA1/2020 virus at a MOI of 2, and viral RNAs from (A) supernatant and (B) cellular fractions were quantified after 72 h of infection. Mean ± SEM of $n = 3$ organoids cultured and infected in different wells, $*p < 0.05$ by Student's $t$-test.

2, and a high expression of both ACE2 and TMPRSS2 and were verified to permit SARS-CoV-2 infection as described previously.[38−40] Organoids were pretreated with 5 $\mu$M E24 for 2 h and infected with SARS-CoV-2 at MOI = 2 for 2 h at 37 °C. Then, the cells were washed, and a fresh medium was added. At 72 h postinfection, both intracellular viral RNA and viral RNA from the supernatant were isolated and quantified by RT-qPCR. As shown in Figure 4, E24 treatment reduced viral RNA levels by ∼50% in both the supernatant and intracellular fractions with no observable toxicity toward the organoids. These data confirm that E24 can impair the viral replication of SARS-CoV-2 in human lung organoids.

## DISCUSSION AND CONCLUSIONS

In this study, we sought to apply medicinal chemistry and rational drug design approaches to the SARS-CoV-2 main protease to address the following specific goals: (1) to improve potency of early M$^{pro}$ screening hits, (2) to establish an enzymatic mechanism of inhibition, (3) to rationally design compounds with potent antiviral activity, and (4) to compare rationally designed compounds against existing early SARS-CoV-2 antivirals. With this approach, we have identified a class of 2-phenyl-1,2-benzoselenazol-3-one compounds showing nanomolar potencies against recombinant SARS-CoV-2 M$^{pro}$ and improved lipophilicities relative to the early M$^{pro}$ inhibitor ebselen. Using steady-state enzyme kinetics, we were able to establish that some 2-phenyl-1,2-benzoselenazol-3-one compounds inhibit M$^{pro}$ noncovalently, suggesting they are less likely to suffer from target promiscuity than covalent modifiers such as ebselen. Furthermore, lead compound E04 was found to inhibit M$^{pro}$ through a competitive mechanism of inhibition, indicating that nonpeptidyl small molecules may bind to the active site of M$^{pro}$ to inhibit proteolysis. Additionally, 2-phenyl-1,2-benzoselenazol-3-one compounds were determined to inhibit SARS-CoV-2 viral replication in infected Vero E6 and Calu-3 cells with comparable potencies to that of the clinical treatment remdesivir. The further evaluation of lead E24 in iPSC-derived human lung organoids confirmed that E24 was able to significantly reduce viral RNA levels in both supernatant and intracellular fractions at a 5 $\mu$M dose.

Ebselen is known to be a promiscuous protease inhibitor capable of binding a variety of viral proteases, including SARS-CoV-2 M$^{pro}$ and PL$^{pro}$, EV-A71 2A$^{pro}$ and 3C$^{pro}$, and EV-D68 2A$^{pro}$ and 3C$^{pro}$.[41,42] At this stage, it is unknown if the 2-phenyl-1,2-benzoselenazol-3-one analogues presented in this study are also able to bind and inhibit additional proteases such as the SARS-CoV-2 papain-like protease (PL$^{pro}$), which cleaves nonstructural protein 1 (nsp1), nonstructural protein 2 (nsp2), and nonstructural protein 3 (nsp3) of the viral polyprotein. PL$^{pro}$ has been identified as a promising drug target for SARS-CoV-2 both for its essential role in promoting viral replication and also for its ability to promote immune escape by cleaving the host ubiquitin-like interferon-stimulated gene 15 protein (ISG15), a key regulator of the host innate immune response.[43−46] Without further studies to characterize the selectivity index of the 2-phenyl-1,2-benzoselenazol-3-one inhibitors, we cannot say if the antiviral activity observed in both the Vero E6 and Calu-3 assays and the human iPSC-derived lung organoids is due to the inhibition of M$^{pro}$, PL$^{pro}$, or a combination of both. Additionally, while the mechanism of action has been evaluated for some benzoisoselenazole compounds *in vitro*, it remains unclear if the compounds are covalent or noncovalent modifiers intracellularly. Tandem MS/MS experiments to verify covalent modification at the active site should be completed prior to advancing these compounds as leads for clinical development. However, we believe that while E24 shows promise as a M$^{pro}$ inhibitor, and the potency can be further optimized prior to establishing the selectivity and intracellular mechanism of action of this class of inhibitors.

While future studies are needed to determine toxicity and efficacy of the 2-phenyl-1,2-benzoselenazol-3-one class of compounds in animal models, these findings could potentially be relevant to the development of M$^{pro}$-targeted clinical candidates for the treatment of COVID-19.

## EXPERIMENTAL SECTION

***In Silico* Modeling of Ebselen Analogues with Schrödinger.** *In silico* modeling of ebselen analogs was performed using the Glide docking module of the Schrödinger 11.5 modeling software suite. A crystal structure of the SARS-CoV-2 $^{pro}$ bound to N3 (PDB ID 6UL7) was first refined using Prime.[15,47,48] The optimized potentials for liquid simulations (OPLS) all-atom force field and the surface generalized born (SGB) continuum solution model were used to optimize and minimize the crystal structure, respectively. The docking grid was generated as a 15 Å cube centered on N3 ($x = -14$, $y = 17.7$, and $z = 67.1$). Ligprep was used to generate a minimized 3D structure for all antiviral compounds using the OPLS 2001 force field. Docking was performed with Glide XP.[21−23] Compounds were ranked by their docking score, and the docking poses were evaluated for interactions with key residues such as the catalytic dyad His 41 and Cys 145.

**SARS-CoV-2 Main Protease Protein Expression and Purification.** The GST-tagged SARS-CoV-2 main protease was expressed in *Escherichia coli* BL21 competent cells (New England Biolabs), which were transformed with the pET41b plasmid by heat shock and

spread on a lysogeny broth (LB) kanamycin agar plate and then incubated overnight at 37 °C. Next, 2−3 colonies were picked and transferred to 5 mL of LB medium treated with kanamycin (0.5 mg/mL final concentration), then grown overnight with shaking at 37 °C. The overnight culture was then transferred to 2 L of the LB kanamycin medium and incubated at 37 °C until OD = 0.8. The culture was cooled at 4 °C for 20 min, induced with 0.5 mM isopropyl β-D-1-thiogalactopyranoside (IPTG), then grown with shaking at 16 °C. Cell pellets were collected by centrifugation (5000 $g$ for 10 min at 4 °C), and the supernatant was discarded. The pellets were resuspended in lysis buffer (50 mM Tris-HCl pH 7.5, 500 mM NaCl, 1.0% Triton x-100, 0.5 mM EDTA, 1× complete protease inhibitor cocktail, and 1 mM β-mercaptoethanol in RNase-free water; 6 mL per gram) with DNase 1 (5 U/mL, RNase-free) and incubated at 4 °C for 1 h, then sonicated. The suspension was centrifuged at 10 000 $g$ for 20 min, and the supernatant was transferred to a glutathione sepharose affinity resin column that had been pre-equilibrized with lysis buffer. The supernatant was incubated with the affinity resin column at 4 °C for 2 h with end-over-end rotation. After incubation, the column was washed with 5 bed volumes of lysis buffer, 3 × 5 bed volumes of wash buffer (50 mM Tris-HCl pH 7.5, 500 mM NaCl, 0.1% Triton x-100, 0.5 mM EDTA, 1× complete protease inhibitor cocktail, and 1 mM β-mercaptoethanol in RNase-free water), and 5 bed volumes of pre-elution buffer (50 mM Tris-HCl pH 7.5 and 100 mM NaCl in RNase-free water). The protease was eluted with elution buffer (50 mM Tris-HCl pH 7.5, 100 mM NaCl, and 40 mM glutathione in RNase-free water) and collected in 1 mL fractions until no further protein was collected (3−5 bed volumes total). The purity of the fractions was determined by SDS-page, and fractions of the purified protein were collected and concentrated to 2 mg/mL. The GST-tagged purified protein was incubated with TEV protease at 37 °C for 4 h to obtain the untagged SARS-CoV-2 protease. Excess GST and GST-TEV protease were removed by glutathione sepharose affinity column purification. The untagged proteases were eluted in 50 mM Tris-HCl pH 7.5 and 100 mM NaCl in RNase-free water. The purity of the fractions was determined by SDS-page, and fractions of purified protein were collected and concentrated to 5 μM. The protein solutions were transferred to a Slyde-A-Lyzer dialysis cassette (20 000 MWCO, Thermo Scientific) and dialyzed overnight at 4 °C against dialysis buffer (50 mM Tris-HCl pH 7.4, 200 mM NaCl, 1 mM EDTA, and 1 mM DTT in RNase-free water).
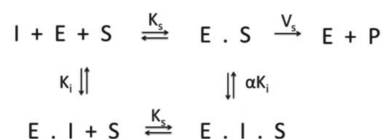
**FRET Protease Activity Assay.** The activity of the SARS-CoV-2 main proteases was determined using a fluorescence resonance energy transfer (FRET) assay adapted from Muramatsu et al.[25] The fluorogenic peptide Dabcyl-Val-Asn-Ser-Thr-Leu-Gln-Ser-Gly-Leu-Arg-Lys-EDANS was used as a substrate (AnaSpec Inc.). All reactions were performed in a black 96-well plate with 200 μL of assay buffer (50 mM Tris-HCl pH 7.4, 200 mM NaCl, 1 mM EDTA, and 1 mM DTT in RNase-free water), 25 nM SARS-CoV-2 protease, and 3 μM substrate. Ebselen analogs were screened at a concentration of 10 μM. All inhibitors were dissolved in DMSO and added to a final concentration of 0.2% DMSO. Fluorescent readings were normalized to 200 μL of assay buffer with 3 μM substrate and 10 μM inhibitor with a final concentration of 0.2% DMSO. Cleavage between the Gln and Ser residues was monitored by a BioTek Synergy plate reader with excitation at 380 nm and emission at 485 nm every 10 min for 1 h. The relative rate for wild-type protease, and each inhibitor concentration was averaged from three assay results. The relative reaction rates were normalized to the wild-type protease, and the relative activity was reported as a percentage of the wild-type protease activity in Table 1.

Additionally, dose−response curves were generated for compounds that showed significant inhibition at 10 μM using the assay conditions described above. The dose−response curve for ebselen (E01) was also generated as a positive control. Inhibitors were screened at six concentrations ranging from 0.100 to 10 μM. As before, cleavage between the Gln and Ser residues was monitored by a BioTek Synergy plate reader with excitation at 380 nm and emission at 485 nm every 10 min for 1 h. The relative rates for the wild-type protease and each inhibitor concentration were averaged from three assay results. The

relative reaction rates were normalized to the wild-type protease, and dose−response curves were plotted in GraphPad Prism 6.

To determine if the ebselen analogs were covalent or rapid reversible inhibitors of SARS-CoV-2 M$^{pro}$, preincubation dilution experiments were performed. In assay buffer, 250 nM protease was incubated on ice for 30 min with 10 μM ebselen (E01), E04, E07, E19, E20, or E25. The reaction mixture was then diluted 10-fold with assay buffer, and the fluorogenic peptide substrate was added to a final concentration of 3 μM. The experiment was also repeated with assay buffer free of DTT to determine the effects of the reducing agent on the mechanism of inhibition. For each compound, the rate of product formation after preincubation and dilution was compared to the rate of product formation for M$^{pro}$ with 0.2% DMSO, 1 μM compound, and 10 μM compound without dilution.

**Inhibition Mechanism.** The reaction velocities observed over a range of substrate (1.5, 3, 4.5, 6, 9, 15, 22.5, and 30 μM) and inhibitor concentrations (0, 0.5, 1, 5, and 10 μM) for either ebselen or E04 were globally fit to a generalized mixed-model of inhibition represented by the following equilibrium reaction scheme. This mechanism allows for inhibitor binding to both the free enzyme and the enzyme−substrate complex with varying affinity to be described by the following rate equation: The term $K_i$ describes the affinity of the

$$I + E + S \xrightleftharpoons{K_s} E \cdot S \xrightarrow{V_s} E + P$$

$$K_i \updownarrow \qquad\qquad \updownarrow \alpha K_i$$

$$E \cdot I + S \xrightleftharpoons{K_s} E \cdot I \cdot S$$

inhibitor for free enzyme. The mechanism can be evaluated by the term $\alpha$. When $\alpha$ approaches 1, the inhibitor is considered noncompetitive, and when $\alpha$ approaches infinity, the inhibitor is considered competitive.

$$v_{obs} = \frac{[S]k_{cat}[E]_{total}}{K_m\left(1 + \frac{[I]}{K_i}\right) + [S]\left(1 + \frac{[I]}{\alpha K_i}\right)} \tag{2}$$

**logD Measurements.** logD values were measured at pH 7.4 by the shake-flask method according to the literature.[49,50]

**Antiviral Assays.** Approximately $2 \times 10^4$ Vero E6 cells (ATCC) were plated in 100 μL of DMEM (Gibco) supplemented with 10% serum in each well of a 96-well flat bottom plate and allowed to adhere overnight. Cells were pretreated with 0.10−20 μM test compound in 100 μL of the same medium for 1 h, washed, and infected with SARS-CoV-2 (USA_WA01/2020 (World Reference Center for Emerging Viruses and Arboviruses, University of Texas Medical Branch)) in 50 μL of medium at 0.01 MOI for 1.5 h. Cells were then washed, test compounds were reapplied at 0.10−20 μM in 100 μL of medium, and incubated at 37 °C in 5% $CO_2$ for 72 h. Following incubation, 10 μL of room temperature WST8 reagent was added to each well, mixed, and incubated for an additional 3 h at 37 °C and 5% $CO_2$. The OD at 460 nm was read on a BioTek plate reader.

For antiviral assays in Calu-3 human lung cells, approximately $1.5 \times 10^5$ Calu-3 cells (ATCC) were plated in 500 μL of EMEM (Gibco) supplemented with 10% FBS, 2 mM L-glutamine, and 1% penicillin/streptomycin in each well of 24-well flat bottom plates and allowed to adhere overnight. Cells were pretreated with 0.10−20 μM test compound in DMSO (0.2% final v/v) of the same medium for 1 h, washed, and infected with SARS-CoV-2 (USA_WA01/2020) in a reduced serum medium (2−3%) at 0.1 MOI for 1.5 h. Cells were then washed with PBS, and test compounds reapplied at 0.10−20 μM in 500 μL of the medium and incubated at 37 °C in 5% $CO_2$ for 24 h. At 24 h postinfection, the supernatant and infected cells were collected and lysed using TRIzol, and RNA was extracted using a Direct-zol RNA Kit (Zymo) and quantified by RT-qPCR using SARS-CoV-2 N primers as previously described.[38−40] The primers are as follows: forward, CACATTGGCACCCGCAATC; reverse, GAGGA-ACGAGAAGAGGCTTG.

**Lung Organoid Infection and Treatment with E24.** Human iPSC-derived lung organoids were generated using previously published methods and characterized by the expression of ACE2, TMPRSS2, and alveolar cell epithelial markers (SFTPC, SFTPB, and HOPX). The 60D differentiated lung organoids were pretreated with 5 μM E24 for 2 h and infected with SARS-CoV-2 as described previously.[38] The SARS-CoV-2 isolate USA-WA1/2020 was obtained from BEI Resources. SARS-CoV-2 was propagated, and infectious units quantified by plaque assay using Vero E6 cells. Human iPSC-derived lung organoids, were infected with SARS-CoV-2 at MOI = 2 for 2 h at 37 °C. Then, cells were washed, and fresh medium was added. At 72 h post infection, the supernatant and infected organoids were collected and lysed using TRIzol, and RNA was extracted using a Direct-zol RNA kit (Zymo) and quantified by RT-qPCR using SARS-CoV-2 N primers.

**General Procedure for the Synthesis of Compounds E01−30.** A one-necked round-bottomed flask was fitted with a reflux condenser and a magnetic stirrer. The flask was charged with the corresponding SM 3 (1 mmol), followed by the addition of Se powder (5 mmol) and tBuONa (2 mmol). The reaction mixture was left to stir at 130 °C for 12 h. After the completion of reaction, the reaction mixture was diluted with excess water and extracted with ethyl acetate. The organic layer was separate and concentrated under reduced pressure. The crude material was purified by column chromatography (hexane/ethyl acetate 70:30) to yield compounds E01−30 as solids.

**Compound Characterization.** The Supporting Information provides a detailed description of the solvent purification and general methods for synthesis and purification of each analogue. All compounds were purified by column chromatography and characterized by $^1$H and $^{13}$C NMR and HRMS. Purity was determined by HPLC at >90% for all compounds, and spectra can be found in the Supporting Information.

*2-Phenylbenzo[d][1,2]selenazol-3(2H)-one (E01).* $^1$H NMR (600 MHz, CDCl$_3$) δ 8.17 (d, J = 7.8 Hz, 1H), 7.72 (t, J = 7.8 Hz, 1H), 7.69 (dd, J = 8.4, 2.8 Hz, 3H), 7.52 (td, J = 6.2, 1.3 Hz, 1H), 7.48 (t, J = 8.4 Hz, 2H), 7.33 (dd, J = 14.1, 6.6 Hz, 1H). $^{13}$C NMR (151 MHz, CDCl$_3$) δ 165.8, 139.2, 137.7, 132.6, 132.6, 129.5, 129.4, 127.6, 126.8, 126.6, 125.5, 125.5, 123.8. HRMS (ESI): m/z calculated for C$_{13}$H$_9$NOSe 274.9849, found 275.9927 [M + H]$^+$. Purity >99%.

*2-(4-Fluorophenyl)benzo[d][1,2]selenazol-3(2H)-one (E02).* $^1$H NMR (600 MHz, CDCl$_3$) δ 8.11 (d, J = 7.8 Hz, 1H), 7.68−7.64 (m, 2H), 7.57 (dd, J = 8.6, 4.8 Hz, 2H), 7.48 (t, J = 6.6 Hz, 1H), 7.12 (t, J = 8.5 Hz, 2H). $^{13}$C NMR (151 MHz, CDCl$_3$) δ 165.9, 161.9, 160.3, 137.7, 134.9, 132.7, 129.5, 127.7, 127.1, 126.7, 123.9, 116.3, 116.2. HRMS (ESI): m/z calculated for C$_{13}$H$_8$FNOSe 292.9755, found 293.9831[M + H]$^+$. Purity >99%.

*2-(2-(Methylthio)phenyl)benzo[d][1,2]selenazol-3(2H)-one (E03).* $^1$H NMR (600 MHz, CDCl$_3$) δ 8.19 (d, J = 7.8 Hz, 1H), 7.75−7.68 (m, 2H), 7.52 (t, J = 7.3 Hz, 1H), 7.47−7.41 (m, 2H), 7.37 (d, J = 8.0 Hz, 1H), 7.28 (t, J = 7.6 Hz, 1H), 2.48 (s, 3H). $^{13}$C NMR (151 MHz, CDCl$_3$) δ 165.9, 138.8, 138.5, 134.8, 132.0, 129.4, 129.0, 129.0, 125.8, 125.7, 125.5, 125.0, 123.5, 14.6. HRMS (ESI): m/z calculated for C$_{14}$H$_{11}$NOSSe 320.9727, found 321.9805 [M + H]$^+$. Purity >98%.

*2-(4-(Trifluoromethyl)phenyl)benzo[d][1,2]selenazol-3(2H)-one (E04).* $^1$H NMR (600 MHz, CDCl$_3$) δ 8.13 (d, J = 7.8 Hz, 1H), 7.81 (d, J = 8.4 Hz, 2H), 7.70−7.67 (m, 4H), 7.49 (ddd, J = 8.0, 5.6, 2.6 Hz, 1H). $^{13}$C NMR (151 MHz, CDCl$_3$) δ 167.0, 137.3, 133.2, 133.2, 129.7, 129.7, 127.4, 127.0, 127.0, 126.7, 126.6, 124.9, 123.9, 123.9. HRMS (ESI): m/z calculated for C$_{14}$H$_8$F$_3$NOSe 342.9723, found 343.9798 [M + H]$^+$. Purity >98%.

*2-(3,4-Dimethylphenyl)benzo[d][1,2]selenazol-3(2H)-one (E05).* $^1$H NMR (600 MHz, CDCl$_3$) δ 8.16 (d, J = 7.6 Hz, 1H), 7.69 (dt, J = 7.9, 7.3 Hz, 2H), 7.51 (t, J = 7.3 Hz, 1H), 7.45 (s, 1H), 7.36 (d, J = 8.0 Hz, 1H), 7.23 (d, J = 8.0 Hz, 1H), 2.35 (s, 3H), 2.32 (s, 3H). $^{13}$C NMR (151 MHz, CDCl$_3$) δ 165.8, 137.8, 137.8, 136.6, 135.8, 132.4, 130.4, 129.4, 127.6, 126.8, 126.5, 123.8, 123.1, 19.9, 19.5. HRMS (ESI): m/z calculated for C$_{15}$H$_{13}$NOSe 303.0162, found 304.0240 [M + H]$^+$. Purity >98%.

*2-(4-Fluorobenzyl)benzo[d][1,2]selenazol-3(2H)-one (E06).* $^1$H NMR (600 MHz, CDCl$_3$) δ 8.13 (d, J = 7.8 Hz, 1H), 7.63 (t, J = 6.4 Hz, 2H), 7.48 (td, J = 8.0, 4.2 Hz, 1H), 7.39 (dd, J = 8.0, 5.5 Hz, 2H), 7.10 (t, J = 8.5 Hz, 2H), 5.03 (s, 2H). $^{13}$C NMR (151 MHz, CDCl$_3$) δ 167.3, 163.6, 161.0, 138.1, 133.2, 132.3, 130.5, 130.4, 129.1, 126.5, 124.2, 116.09, 115.9, 48.0. HRMS (ESI): m/z calculated for C$_{14}$H$_{10}$FNOSe 306.9912, found 307.9988 [M + H]$^+$. Purity >99%.

*2-(2,4-Dimethoxybenzyl)benzo[d][1,2]selenazol-3(2H)-one (E07).* $^1$H NMR (600 MHz, CDCl$_3$) δ 8.04 (d, J = 7.9 Hz, 1H), 7.54−7.51 (m, 2H), 7.39 (qd, J = 5.8, 3.0 Hz, 1H), 7.32 (d, J = 8.2 Hz, 1H), 6.46 (dt, J = 8.2, 2.2 Hz, 2H), 4.96 (s, 2H), 3.87 (d, J = 6.7 Hz, 3H), 3.81 (s, 3H). $^{13}$C NMR (151 MHz, CDCl$_3$) δ 167.0, 161.3, 158.7, 138.5, 131.9, 131.7, 128.7, 127.9, 126.0, 123.8, 118.2, 104.4, 98.6, 55.5, 55.5, 43.2. HRMS (ESI): m/z calculated for C$_{16}$H$_{15}$NO$_3$Se 349.0217, found 350.0296 [M + H]$^+$. Purity >98%.

*2-(2-Fluorophenyl)benzo[d][1,2]selenazol-3(2H)-one (E08).* $^1$H NMR (600 MHz, CDCl$_3$) δ 8.19 (d, J = 7.8 Hz, 1H), 7.72 (d, J = 8.2 Hz, 2H), 7.55 (ddd, J = 8.0, 5.6, 2.6 Hz, 2H), 7.45−7.39 (m, 1H), 7.30−7.23 (m, 2H). $^{13}$C NMR (151 MHz, CDCl$_3$) δ 166.6, 159.2, 157.5, −139.1, 132.8, 130.3, 130.1, 130.0, 129.6, 126.6, 124.8, 124.1, 117.1. HRMS (ESI): m/z calculated for C$_{13}$H$_8$FNOSe 292.9755, found 293.9834 [M + H]$^+$. Purity >99%.

*2-(4-(Trifluoromethyl)benzyl)benzo[d][1,2]selenazol-3(2H)-one (E09).* $^1$H NMR (600 MHz, CDCl$_3$) δ 8.15 (d, J = 7.8 Hz, 1H), 7.69−7.65 (m, 4H), 7.51 (t, J = 8.1 Hz, 3H), 5.13 (s, 2H). $^{13}$C NMR (151 MHz, CDCl$_3$) δ 167.5, 137.8, 132.5, 129.3, 129.3, 128.7, 128.7, 126.9, 126.6, 126.6, 126.0, 126.0, 124.2, 124.2, 48.1. HRMS (ESI): m/z calculated for C$_{15}$H$_{10}$F$_3$NOSe 356.9880, found 357.9957 [M + H]$^+$. Purity >99%.

*2-(4-Fluoro-2-(trifluoromethyl)phenyl)benzo[d][1,2]selenazol-3(2H)-one (E10).* $^1$H NMR (600 MHz, CDCl$_3$) δ 8.28 (d, J = 3.5 Hz, 1H), 8.05 (s, 1H), 7.79 (d, J = 7.8 Hz, 1H), 7.64 (d, J = 7.5 Hz, 1H), 7.51−7.47 (m, 1H), 7.44−7.40 (m, 2H). $^{13}$C NMR (151 MHz, CDCl$_3$) δ 166.4, 160.1, 135.2, 133.7, 132.3, 132.2, 130.9, 127.7, 127.3, 127.1, 126.6, 120.1, 119.9, 113.8. HRMS (ESI): m/z calculated for C$_{14}$H$_7$F$_4$NOSe 360.9629, found 361.9704 [M + H]$^+$. Purity >90%.

*2-(2,6-Difluorophenyl)benzo[d][1,2]selenazol-3(2H)-one (E11).* $^1$H NMR (600 MHz, CDCl$_3$) δ 8.15 (d, J = 7.7 Hz, 1H), 7.82 (d, J = 7.4 Hz, 1H), 7.74 (s, 1H), 7.472 (d, J = 7.0 Hz, 1H), 7.38 (m, 1H), 7.06 (m, 2H). $^{13}$C NMR (151 MHz, CDCl$_3$) δ 169.7, 166.7, 139.6, 133.5, 133.0, 132.2, 130.4, 129.7, 129.1, 126.6, 124.2, 112.5, 112.3. HRMS (ESI): m/z calculated for C$_{13}$H$_7$F$_2$NOSe 310.9661, found 311.9737 [M + H]$^+$. Purity >90%.

*2-(4-Methoxybenzyl)benzo[d][1,2]selenazol-3(2H)-one (E12).* $^1$H NMR (600 MHz, CDCl$_3$) δ 8.12 (d, J = 7.8 Hz, 1H), 7.61 (d, J = 3.6 Hz, 2H), 7.50−7.45 (m, 1H), 7.35 (dt, J = 8.6, 2.1 Hz, 2H), 6.94 (dt, J = 8.6, 1.9 Hz, 2H), 5.00 (s, 2H), 3.86 (d, J = 6.4 Hz, 3H). $^{13}$C NMR (151 MHz, CDCl$_3$) δ 167.1, 159.7, 138.2, 131.9, 130.2, 130.2, 129.4, 128.9, 127.8, 126.2, 124.0, 114.2, 114.2, 55.4, 48.3. HRMS (ESI): m/z calculated for C$_{15}$H$_{13}$NO$_2$Se 319.0112, found 320.0190 [M + H]$^+$. Purity >99%.

*2-(4-Chloro-2-(trifluoromethoxy)phenyl)benzo[d][1,2]selenazol-3(2H)-one (E13).* $^1$H NMR (600 MHz, CDCl$_3$) δ 8.54 (d, J = 8.8 Hz, 1H), 8.18 (s, 1H), 7.78 (d, J = 7.8 Hz, 1H), 7.64 (dd, J = 7.6, 1.1 Hz, 1H), 7.48 (td, J = 7.7, 1.4 Hz, 1H), 7.42 (dd, J = 7.5, 0.6 Hz, 1H), 7.37−7.35 (m, 1H). $^{13}$C NMR (151 MHz, CDCl$_3$) δ 166.0, 138.6, 135.4, 133.3, 132.4, 132.3, 129.6, 129.0, 127.8, 127.4, 127.3, 122.9, 120.8, 46.0. HRMS (ESI): m/z calculated for C$_{14}$H$_7$ClF$_3$NO$_2$Se 392.9283, found 393.9352 [M + H]$^+$. Purity >95%.

*2-(5-Chloro-2-methoxyphenyl)benzo[d][1,2]selenazol-3(2H)-one (E14).* $^1$H NMR (600 MHz, CDCl$_3$) δ 8.17 (d, J = 7.4 Hz, 1H), 7.70 (t, J = 5.9 Hz, 2H), 7.56 (d, J = 2.4 Hz, 1H), 7.53−7.49 (m, 1H), 7.39−7.35 (m, 1H), 6.99 (d, J = 8.9 Hz, 1H), 3.89 (s, 3H). $^{13}$C NMR (151 MHz, CDCl$_3$) δ 166.8, 154.1, 139.2, 132.6, 129.9, 129.5, 129.5, 127.9, 126.4, 126.1, 125.5, 123.9, 113.4, 56.3. HRMS (ESI): m/z calculated for C$_{14}$H$_{10}$ClNO$_2$Se 338.9565, found 339.9641 [M + H]$^+$. Purity >93%.

*2-(4-Chlorophenyl)benzo[d][1,2]selenazol-3(2H)-one (E15).* $^1$H NMR (600 MHz, (CD$_3$)$_2$SO) δ 8.08 (d, J = 8.0 Hz, 1H), 7.91 (dd, J = 7.8, 1.4 Hz, 2H), 7.68 (t, J = 7.7 Hz, 1H), 7.48 (t, J = 7.4 Hz, 1H), 7.36 (t, J = 8.2 Hz, 1H), 7.31 (t, J = 2.3 Hz, 1H), 7.16 (dd, J = 7.8, 1.2 Hz, 1H), 6.86 (dd, J = 8.3, 2.5 Hz, 1H), 3.79 (s, 3H). $^{13}$C NMR (151

MHz, $(CD_3)_2SO$) $\delta$ 165.0, 159.7, 140.9, 138.9, 132.3, 130.0, 128.6, 128.0, 126.3, 125.8, 116.7, 111.4, 110.4, 55.3. HRMS (ESI): $m/z$ calculated for $C_{14}H_{11}NO_2Se$ 304.9955, found 309.3315 [M + H]$^+$. Purity >90%.

*2-(5-Fluoro-2-methoxyphenyl)benzo[d][1,2]selenazol-3(2H)-one* **(E16)**. $^1$H NMR (600 MHz, CDCl$_3$) $\delta$ 8.12 (d, $J$ = 7.7 Hz, 1H), 7.66–7.63 (m, 2H), 7.45 (ddd, $J$ = 8.1, 5.7, 2.4 Hz, 1H), 7.33 (dd, $J$ = 8.7, 2.8 Hz, 1H), 7.05 (td, $J$ = 8.5, 3.1 Hz, 1H), 6.94 (dd, $J$ = 9.0, 4.8 Hz, 1H), 3.84 (s, 3H). $^{13}$C NMR (151 MHz, CDCl$_3$) $\delta$ 166.3, 156.6, 155.0, 151.9, 140.8, 132.7, 132.5, 128.2, 127.4 126.2, 116.7, 115.3, 114.0, 56.6. HRMS (ESI): $m/z$ calculated for $C_{14}H_{10}FNO_2Se$ 322.9861, found 323.9937 [M + H]$^+$. Purity >99%.

*2-(4-Fluoro-2-methoxyphenyl)benzo[d][1,2]selenazol-3(2H)-one* **(E17)**. $^1$H NMR (600 MHz, CD$_3$OD) $\delta$ 8.07 (d, $J$ = 8.0 Hz, 1H), 7.86 (d, $J$ = 7.3 Hz, 1H), 7.67 (ddd, $J$ = 8.3, 7.2, 1.5 Hz, 1H), 7.46 (td, $J$ = 7.5, 1.0 Hz, 1H), 7.37 (dd, $J$ = 8.6, 6.4 Hz, 1H), 7.11 (dd, $J$ = 11.0, 2.6 Hz, 1H), 6.85 (td, $J$ = 8.4, 2.7 Hz, 1H), 3.78 (s, 3H). $^{13}$C NMR (151 MHz, CD$_3$OD) $\delta$ 166.3, 140.9, 132.5, 131.5, 128.3, 127.6, 126.4, 126.4, 107.3, 107.1, 101.4, 101.3, 56.7, 36.3. HRMS (ESI): $m/z$ calculated for $C_{14}H_{10}FNO_2Se$ 322.9861, found 323.9938 [M + H]$^+$. Purity >95%.

*2-(4-Ethylphenyl)benzo[d][1,2]selenazol-3(2H)-one* **(E18)**. $^1$H NMR (600 MHz, CDCl$_3$) $\delta$ 8.12 (d, $J$ = 7.7 Hz, 1H), 7.67–7.63 (m, 2H), 7.52 (dt, $J$ = 8.2, 2.1 Hz, 2H), 7.47 (ddd, $J$ = 7.9, 6.4, 1.8 Hz, 1H), 7.26 (d, $J$ = 8.2 Hz, 2H), 2.67 (q, $J$ = 7.6 Hz, 2H), 1.26 (t, $J$ = 7.6 Hz, 3H). $^{13}$C NMR (151 MHz, CDCl$_3$) $\delta$ 165.8, 143.2, 137.8, 136.6, 132.5, 129.4, 128.8, 128.8, 127.6, 126.5, 125.6, 125.6, 123.8, 28.5, 15.6. HRMS (ESI): $m/z$ calculated for $C_{15}H_{13}NOSe$ 303.0162, found 304.0240 [M + H]$^+$. Purity >99%.

*2-(3-Chlorophenyl)benzo[d][1,2]selenazol-3(2H)-one* **(E19)**. $^1$H NMR (600 MHz, CDCl$_3$ + CD$_3$OD) $\delta$ 7.92 (d, $J$ = 7.6 Hz, 1H), 7.69 (d, $J$ = 8.0 Hz, 1H), 7.53 (dt, $J$ = 8.2, 1.6 Hz, 2H), 7.35 (dd, $J$ = 8.0, 1.1 Hz, 1H), 7.34 (t, $J$ = 7.0 Hz, 1H), 7.24 (d, $J$ = 8.0 Hz, 1H), 7.14 (ddd, $J$ = 7.2, 4.0, 3.2 Hz, 1H). $^{13}$C NMR (151 MHz, CDCl$_3$) $\delta$ 166.4, 140.1, 138.6, 134.7, 132.7, 130.2, 128.8, 127.3, 126.8, 126.5, 125.5, 124.3, 123.5. HRMS (ESI): $m/z$ calculated for $C_{13}H_8ClNOSe$ 308.9460, found 309.9536 [M + H]$^+$. Purity >98%.

*2-(3,5-Dichlorophenyl)benzo[d][1,2]selenazol-3(2H)-one* **(E20)**. $^1$H NMR (600 MHz, $(CD_3)_2SO$) $\delta$ 8.11–8.06 (m, 2H), 7.91 (d, $J$ = 2.2 Hz, 1H), 7.69 (t, $J$ = 7.6 Hz, 2H), 7.58 (dd, $J$ = 8.3, 2.7 Hz, 1H), 7.48 (t, $J$ = 7.5 Hz, 1H). $^{13}$C NMR (151 MHz, $(CD_3)_2SO$) $\delta$ 166.4, 140.1, 138.6, 134.7, 132.7, 130.2, 128.8, 127.3, 126.8, 126.5, 125.5, 124.3, 123.54. HRMS (ESI): $m/z$ calculated for $C_{13}H_7Cl_2NOSe$ 342.9070, found 344.2213 [M + H]$^+$. Purity >95%.

*2-(4-Bromophenyl)benzo[d][1,2]selenazol-3(2H)-one* **(E21)**. $^1$H NMR (600 MHz, CD$_3$OD + CDCl$_3$) $\delta$ 8.12 (d, $J$ = 7.9 Hz, 1H), 7.90 (dd, $J$ = 7.8, 1.4 Hz, 1H), 7.69 (ddd, $J$ = 8.3, 7.2, 1.4, Hz, 1H), 7.64 (s, 4H), 7.48 (td, $J$ = 7.5, 1.1 Hz, 1H). $^{13}$C NMR (151 MHz, CDCl$_3$) $\delta$ 165.1, 139.3, 138.6, 132.4, 132.0, 132.0, 128.5, 128.0, 126.4, 126.4, 126.4, 126.1, 117.8. HRMS (ESI): $m/z$ calculated for $C_{13}H_8BrNOSe$ 352.8954, found 353.9028 [M + H]$^+$. Purity >95%.

*2-(p-Tolyl)benzo[d][1,2]selenazol-3(2H)-one* **(E22)**. 1H NMR (600 MHz,$(CD_3)_2SO$) $\delta$ 8.11 (d, $J$ = 8.1 Hz, 1H), 7.789 (dd, $J$ = 7.8, 1.4 Hz, 1H), 7.67 (t, $J$ = 7.4 Hz, 1H), 7.51 (d, $J$ = 8.1 Hz, 1H), 7.47 (t, $J$ = 7.2 Hz, 2H), 7.25 (d, $J$ = 8.1 Hz, 2H), 2.32 (s, 3H). $^{13}$C NMR (151 MHz, $(CD_3)_2SO$) $\delta$ 164.9, 138.8, 137.1, 135.3, 132.1, 129.6, 129.6, 128.6, 127.9, 126.2, 125.9, 124.7, 124.7, 20.6. HRMS (ESI): $m/z$ calculated for $C_{14}H_{11}NOSe$ 289.0006, found 290.0087 [M + H]$^+$. Purity >96%.

*2-(o-Tolyl)benzo[d][1,2]selenazol-3(2H)-one* **(E23)**. $^1$H NMR (600 MHz, CDCl$_3$) $\delta$ 8.18 (d, $J$ = 7.8 Hz, 1H), 7.74 (t, $J$ = 7.2 Hz, 1H), 7.70 (t, $J$ = 7.5 Hz, 1H), 7.53 (t, $J$ = 7.5 Hz, 1H), 7.38–7.34 (m, 3H), 7.32 (d, $J$ = 5.5 Hz, 1H), 2.29 (s, 3H). $^{13}$C NMR (151 MHz, CDCl$_3$) $\delta$ 166.2, 139.1, 139.1, 137.7, 136.8, 132.4, 131.3, 129.4, 129.2, 129.1, 126.9, 126.5, 124.2, 18.3. HRMS (ESI): $m/z$ calculated for $C_{14}H_{11}NOSe$ 289.0006, found 290.0086 [M + H]$^+$. Purity >98%.

*2-(3-(Trifluoromethyl)phenyl)benzo[d][1,2]selenazol-3(2H)-one* **(E24)**. $^1$H NMR (600 MHz, CDCl$_3$) $\delta$ 8.13 (d, $J$ = 7.9 Hz, 1H), 7.95 (s, 1H), 7.84 (d, $J$ = 7.8 Hz, 1H), 7.68 (d, $J$ = 4.2 Hz, 2H), 7.56 (t, $J$ = 7.8 Hz, 1H), 7.53 (d, $J$ = 7.9 Hz, 1H), 7.49 (ddd, $J$ = 8.0, 4.8, 3.4 Hz, 1H). $^{13}$C NMR (151 MHz, CDCl$_3$) $\delta$ 166.0, 139.9, 137.4, 133.1, 130.1, 129.7, 128.6, 127.0, 127.0, 124.0, 123.4, 123.3, 122.2, 122.2. HRMS (ESI): $m/z$ calculated for $C_{14}H_8F_3NOSe$ 342.9723, found 343.9800 [M + H]$^+$. Purity >99%.

*3-(3-Oxobenzo[d][1,2]selenazol-2(3H)-yl)benzonitrile* **(E25)**. $^1$H NMR (600 MHz, CDCl$_3$) $\delta$ 8.15 (dt, $J$ = 7.8, 1.1 Hz,1H), 7.78 (dd, $J$ = 7.8, 1.4 Hz, 1H), 7.73–7.65 (m, 3H), 7.55 (dd, $J$ = 8.1, 1.1 Hz, 1H), 7.50 (tdd, $J$ = 6.1, 4.6, 2.9 Hz, 2H). $^{13}$C NMR (151 MHz, CDCl$_3$) $\delta$ 166.5, 140.9, 138.6, 134.0, 133.8, 133.2, 129.9, 129.9, 128.7, 126.9, 125.4, 124.1, 116.1, 113.4. HRMS (ESI): $m/z$ calculated for $C_{14}H_8N_2OSe$ 299.9802, found 300.9880 [M + H]$^+$. Purity >98%.

*2-(3-Methoxyphenyl)benzo[d][1,2]selenazol-3(2H)-one* **(E26)**. $^1$H NMR (600 MHz, CDCl$_3$) $\delta$ 8.11 (d, $J$ = 7.8 Hz, 1H), 7.65 (ddd, $J$ = 10.0, 9.1, 4.4 Hz, 2H), 7.46 (ddd, $J$ = 8.0, 6.8, 1.4 Hz, 1H), 7.360–7.28 (m, 2H), 7.16 (ddd, $J$ = 7.9, 2.1, 0.9 Hz, 1H), 6.83 (dd, $J$ = 8.1, 2.3 Hz, 1H), 3.84 (s, 3H). $^{13}$C NMR (151 MHz, CDCl$_3$) $\delta$ 165.8, 160.3, 140.3, 137.82, 132.7, 130.1, 129.5, 127.8, 126.7, 123.8, 117.6, 113.0, 111.0, 55.6. HRMS (ESI): $m/z$ calculated for $C_{14}H_{11}NO_2Se$ 304.9955, found 306.0034 [M + H]$^+$. Purity >99%.

*2-(4-Methoxyphenyl)benzo[d][1,2]selenazol-3(2H)-one* **(E27)**. $^1$H NMR (600 MHz, CDCl$_3$) $\delta$ 8.10 (d, $J$ = 7.7 Hz, 1H), 7.64 (ddd, $J$ = 12.3, 9.0, 4.5 Hz, 2H), 7.49 (d, $J$ = 2. Hz, 1 H), 7.47 (td, $J$ = 6.87, 1.1 Hz, 2H), 6.95 (dt, $J$ = 8.9, 2.2 Hz, 2H), 3.83 (s, 3H). $^{13}$C NMR (151 MHz, CDCl$_3$) $\delta$ 166.1, 158.5, 138.0, 132.4, 131.7, 129.3, 127.5, 127.3, 126.5, 123.9, 123.9, 114.5 114.5, 55.4. HRMS (ESI): $m/z$ calculated for $C_{14}H_{11}NO_2Se$ 304.9955, found 306.0035 [M + H]$^+$. Purity >99%.

*2-Heptylbenzo[d][1,2]selenazol-3(2H)-one* **(E28)**. $^1$H NMR (600 MHz, CDCl$_3$) $\delta$ 8.03 (d, $J$ = 7.8 Hz, 1H), 7.63 (d, $J$ = 7.9 Hz, 1H), 7.57 (td, $J$ = 7.6, 1.4 Hz, 1H), 7.41 (t, $J$ = 7.4 Hz, 1H), 3.84 (t, $J$ = 7.3 Hz, 2H), 1.75–68 (m, 2H), 1.42–1.21 (m, 8H), 0.87 (t, $J$ = 7.0 Hz, 3H). $^{13}$C NMR (151 MHz, CDCl$_3$) $\delta$ 167.1, 137.6, 131.9, 128.9, 127.6, 126.3, 124.0, 44.8, 31.9, 30.4, 28.9, 26.3, 22.8, 14.1. HRMS (ESI): $m/z$ calculated for $C_{14}H_{19}NOSe$ 297.0632, found 298.0711 [M + H]$^+$. Purity >98%.

*2-Octylbenzo[d][1,2]selenazol-3(2H)-one* **(E29)**. $^1$H NMR (600 MHz, CDCl$_3$) $\delta$ 8.04 (d, $J$ = 7.8 Hz, 1H), 7.63 (dt, $J$ = 8.0, 0.9 Hz, 1H), 7.57 (td, $J$ = 7.1, 1.3 Hz, 1H), 7.42 (t, $J$ = 7.2 Hz, 1H), 3.851 (t, $J$ = 7.15 Hz, 2H), 1.72 (m, $J$ = 2H), 1.43–1.27 (m, 4H), 1.29–1.25 (m, 2H), 1.27–1.20 (m, 4 H), 0.87 (t, $J$ = 7.0 Hz, 3H). $^{13}$C NMR (151 MHz, CDCl$_3$) $\delta$ 167.1, 137.7, 131.8, 128.9, 127.7, 126.2, 123.8, 44.9, 31.8, 30.7, 29.3, 29.1, 26.6, 22.6, 14.1. HRMS (ESI): $m/z$ calculated for $C_{15}H_{21}NOSe$ 311.0788, found 312.0868 [M + H]$^+$. Purity >98%.

*2-Pentylbenzo[d][1,2]selenazol-3(2H)-one* **(E30)**. $^1$H NMR (600 MHz, CDCl$_3$) $\delta$ 8.04 (d, $J$ = 7.8 Hz, 1H), 7.63 (d, $J$ = 7.9 Hz, 1H), 7.57 (td, $J$ = 7.7, 1.1 Hz, 1H), 7.42 (t, $J$ = 7.5 Hz, 1H), 3.84 (t, $J$ = 7.3 Hz, 2H), 1.72 (m, 2H), 1.37 (dd, $J$ = 8.7, 5.5 Hz, 4H), 0.90 (t, $J$ = 6.7 Hz, 3H). $^{13}$C NMR (151 MHz, CDCl$_3$) $\delta$ 167.3, 137.7, 131.9, 128.9, 127.7, 126.2, 124.0, 44.9, 30.3, 28.8, 22.4, 14.0. HRMS (ESI): $m/z$ calculated for $C_{12}H_{15}NOSe$ 269.0319, found 270.0398 [M + H]$^+$. Purity >99%.

## ■ ASSOCIATED CONTENT

### ⓈⒾ Supporting Information

The Supporting Information is available free of charge at https://pubs.acs.org/doi/10.1021/acs.jmedchem.1c00566.

> Molecular formula strings(CSV)
>
> Expanded synthetic methods and spectra for E01–30, structures and reported activities for known SARS-CoV-2 main protease inhibitors, docking poses, and individual antiviral dose–response curves for select compounds (PDF)

## ■ AUTHOR INFORMATION

### Corresponding Author

**Tariq M. Rana** − *Division of Genetics, Department of Pediatrics, Center for Drug Discovery Innovation, Program in Immunology, Institute for Genomic Medicine, La Jolla,*

*California 92093, United States; Division of Infectious Diseases and Global Public Health, Department of Medicine, University of California San Diego, La Jolla, California 92093, United States;* ● orcid.org/0000-0001-9558-5766;
Email: trana@ucsd.edu

## Authors

**Sarah Huff** − *Division of Genetics, Department of Pediatrics, Center for Drug Discovery Innovation, Program in Immunology, Institute for Genomic Medicine, La Jolla, California 92093, United States*

**Indrasena Reddy Kummetha** − *Division of Genetics, Department of Pediatrics, Center for Drug Discovery Innovation, Program in Immunology, Institute for Genomic Medicine, La Jolla, California 92093, United States*

**Shashi Kant Tiwari** − *Division of Genetics, Department of Pediatrics, Center for Drug Discovery Innovation, Program in Immunology, Institute for Genomic Medicine, La Jolla, California 92093, United States*

**Matthew B. Huante** − *Department of Microbiology and Immunology, University of Texas Medical Branch, Galveston, Texas 77555, United States*

**Alex E. Clark** − *Division of Infectious Diseases and Global Public Health, Department of Medicine, University of California San Diego, La Jolla, California 92093, United States*

**Shaobo Wang** − *Division of Genetics, Department of Pediatrics, Center for Drug Discovery Innovation, Program in Immunology, Institute for Genomic Medicine, La Jolla, California 92093, United States*

**William Bray** − *Division of Genetics, Department of Pediatrics, Center for Drug Discovery Innovation, Program in Immunology, Institute for Genomic Medicine, La Jolla, California 92093, United States*

**Davey Smith** − *Division of Infectious Diseases and Global Public Health, Department of Medicine, University of California San Diego, La Jolla, California 92093, United States*

**Aaron F. Carlin** − *Division of Infectious Diseases and Global Public Health, Department of Medicine, University of California San Diego, La Jolla, California 92093, United States;* ● orcid.org/0000-0002-1669-8066

**Mark Endsley** − *Department of Microbiology and Immunology, University of Texas Medical Branch, Galveston, Texas 77555, United States*

Complete contact information is available at:
https://pubs.acs.org/10.1021/acs.jmedchem.1c00566

## Author Contributions

[∇]These authors contributed equally to this work. S.H. and I.R.K. designed and performed the experiments, analyzed the data, and wrote the manuscript; S.K.T., M.B.H., A.E.C., S.W., W.B., and M.E. performed experiments and analysis; D.S. provided resources; A.C. gave advice in experimental plans and performed experiments; T.M.R. conceived of and planned the project and participated in experimental design, data analysis, data interpretation, and manuscript writing.

## Notes

The authors declare the following competing financial interest(s): T.M.R. is a founder of ViRx Pharmaceuticals and has an equity interest in the company. The terms of this arrangement have been reviewed and approved by the University of California San Diego in accordance with its conflict of interest policies.

## ■ ABBREVIATONS

ACE2, angiotensin-converting enzyme 2; COVID-19, coronavirus disease 2019; iPSC, induced pluripotent stem cells; ISG15, interferon-stimulated gene 15; MOI, multiplicity of infection; M$^{pro}$, main protease; nsp1, nonstructural protein 1; nsp2, nonstructural protein 2; nsp3, nonstructural protein 3; OPLS, optimized potentials for liquid simulations; PL$^{pro}$, papain-like protease; RT-qPCR, real-time quantitative reverse transcription PCR; RdRp, RNA-dependent RNA polymerase; SARS-CoV-2, severe acute respiratory syndrome coronavirus 2; SGB, surface generalized born; (+)ssRNA, positive-sense single-stranded RNA; TMPRSS2, transmembrane protease serine 2

## ■ REFERENCES

(1) Li, F.; Li, W.; Farzan, M.; Harrison, S. C. Structure of SARS coronavirus spike receptor-binding domain complexed with receptor. *Science* **2005**, *309* (5742), 1864−1868.

(2) Phan, T. Novel coronavirus: From discovery to clinical diagnostics. *Infect., Genet. Evol.* **2020**, *79*, 104211.

(3) Pillaiyar, T.; Manickam, M.; Namasivayam, V.; Hayashi, Y.; Jung, S. H. An Overview of Severe Acute Respiratory Syndrome-Coronavirus (SARS-CoV) 3CL Protease Inhibitors: Peptidomimetics and Small Molecule Chemotherapy. *J. Med. Chem.* **2016**, *59* (14), 6595−628.

(4) Ziebuhr, J.; Snijder, E. J.; Gorbalenya, A. E. Virus-encoded proteinases and proteolytic processing in the Nidovirales. *J. Gen. Virol.* **2000**, *81* (4), 853−879.

(5) Báez-Santos, Y. M.; St. John, S. E.; Mesecar, A. D. The SARS-coronavirus papain-like protease: Structure, function and inhibition by designed antiviral compounds. *Antiviral Res.* **2015**, *115*, 21−38.

(6) Lee, T. W.; Cherney, M. M.; Huitema, C.; Liu, J.; James, K. E.; Powers, J. C.; Eltis, L. D.; James, M. N. Crystal structures of the main peptidase from the SARS coronavirus inhibited by a substrate-like aza-peptide epoxide. *J. Mol. Biol.* **2005**, *353* (5), 1137−1151.

(7) Xu, X.; Liu, Y.; Weiss, S.; Arnold, E.; Sarafianos, S. G.; Ding, J. Molecular model of SARS coronavirus polymerase: implications for biochemical functions and drug design. *Nucleic Acids Res.* **2003**, *31* (24), 7117−7130.

(8) De Clercq, E.; Li, G. Approved Antiviral Drugs over the Past 50 Years. *Clin. Microbiol. Rev.* **2016**, *29* (3), 695−747.

(9) Kanters, S.; Socias, M. E.; Paton, N. I.; Vitoria, M.; Doherty, M.; Ayers, D.; Popoff, E.; Chan, K.; Cooper, D. A.; Wiens, M. O.; Calmy, A.; Ford, N.; Nsanzimana, S.; Mills, E. J. Comparative efficacy and safety of second-line antiretroviral therapy for treatment of HIV/AIDS: A systematic review and network meta-analysis. *Lancet HIV* **2017**, *4* (10), e433−e441.

(10) Deeks, E. D. Darunavir: a review of its use in the management of HIV-1 infection. *Drugs* **2014**, *74* (1), 99−125.

(11) la Porte, C. J. Saquinavir, the pioneer antiretroviral protease inhibitor. *Expert Opin. Drug Metab. Toxicol.* **2009**, *5* (10), 1313−1322.

(12) Heo, Y. A.; Deeks, E. D. Sofosbuvir/Velpatasvir/Voxilaprevir: A Review in Chronic Hepatitis C. *Drugs* **2018**, *78* (5), 577−587.

(13) Sanford, M. Simeprevir: a review of its use in patients with chronic hepatitis C virus infection. *Drugs* **2015**, *75* (2), 183−196.

(14) Chopp, S.; Vanderwall, R.; Hult, A.; Klepser, M. Simeprevir and sofosbuvir for treatment of hepatitis C infection. *Am. J. Health-Syst. Pharm.* **2015**, *72* (17), 1445−1455.

(15) Jin, Z.; Du, X.; Xu, Y.; Deng, Y.; Liu, M.; Zhao, Y.; Zhang, B.; Li, X.; Zhang, L.; Peng, C.; Duan, Y.; Yu, J.; Wang, L.; Yang, K.; Liu, F.; Jiang, R.; Yang, X.; You, T.; Liu, X.; Yang, X.; Bai, F.; Liu, H.; Liu, X.; Guddat, L. W.; Xu, W.; Xiao, G.; Qin, C.; Shi, Z.; Jiang, H.; Rao, Z.; Yang, H. Structure of M(pro) from COVID-19 virus and discovery of its inhibitors. *Nature* **2020**, *582*, 289−293.

(16) Dai, W.; Zhang, B.; Jiang, X. M.; Su, H.; Li, J.; Zhao, Y.; Xie, X.; Jin, Z.; Peng, J.; Liu, F.; Li, C.; Li, Y.; Bai, F.; Wang, H.; Cheng, X.; Cen, X.; Hu, S.; Yang, X.; Wang, J.; Liu, X.; Xiao, G.; Jiang, H.; Rao, Z.; Zhang, L. K.; Xu, Y.; Yang, H.; Liu, H. Structure-based design of antiviral drug candidates targeting the SARS-CoV-2 main protease. *Science* **2020**, *368* (6497), 1331−1335.

(17) Vuong, W.; Khan, M. B.; Fischer, C.; Arutyunova, E.; Lamer, T.; Shields, J.; Saffran, H. A.; McKay, R. T.; van Belkum, M. J.; Joyce, M. A.; Young, H. S.; Tyrrell, D. L.; Vederas, J. C.; Lemieux, M. J. Feline coronavirus drug inhibits the main protease of SARS-CoV-2 and blocks virus replication. *Nat. Commun.* **2020**, *11* (1), 4282.

(18) Zhang, L.; Lin, D.; Sun, X.; Curth, U.; Drosten, C.; Sauerhering, L.; Becker, S.; Rox, K.; Hilgenfeld, R. Crystal structure of SARS-CoV-2 main protease provides a basis for design of improved alpha-ketoamide inhibitors. *Science* **2020**, *368* (6489), 409−412.

(19) Jin, Z.; Zhao, Y.; Sun, Y.; Zhang, B.; Wang, H.; Wu, Y.; Zhu, Y.; Zhu, C.; Hu, T.; Du, X.; Duan, Y.; Yu, J.; Yang, X.; Yang, X.; Yang, K.; Liu, X.; Guddat, L. W.; Xiao, G.; Zhang, L.; Yang, H.; Rao, Z. Structural basis for the inhibition of SARS-CoV-2 main protease by antineoplastic drug carmofur. *Nat. Struct. Mol. Biol.* **2020**, *27* (6), 529−532.

(20) Fu, L.; Ye, F.; Feng, Y.; Yu, F.; Wang, Q.; Wu, Y.; Zhao, C.; Sun, H.; Huang, B.; Niu, P.; Song, H.; Shi, Y.; Li, X.; Tan, W.; Qi, J.; Gao, G. F. Both Boceprevir and GC376 efficaciously inhibit SARS-CoV-2 by targeting its main protease. *Nat. Commun.* **2020**, *11* (1), 4417.

(21) Friesner, R. A.; Banks, J. L.; Murphy, R. B.; Halgren, T. A.; Klicic, J. J.; Mainz, D. T.; Repasky, M. P.; Knoll, E. H.; Shelley, M.; Perry, J. K.; Shaw, D. E.; Francis, P.; Shenkin, P. S. Glide: a new approach for rapid, accurate docking and scoring. 1. Method and assessment of docking accuracy. *J. Med. Chem.* **2004**, *47* (7), 1739−1749.

(22) Halgren, T. A.; Murphy, R. B.; Friesner, R. A.; Beard, H. S.; Frye, L. L.; Pollard, W. T.; Banks, J. L. Glide: a new approach for rapid, accurate docking and scoring. 2. Enrichment factors in database screening. *J. Med. Chem.* **2004**, *47* (7), 1750−1759.

(23) Friesner, R. A.; Murphy, R. B.; Repasky, M. P.; Frye, L. L.; Greenwood, J. R.; Halgren, T. A.; Sanschagrin, P. C.; Mainz, D. T. Extra precision glide: docking and scoring incorporating a model of hydrophobic enclosure for protein-ligand complexes. *J. Med. Chem.* **2006**, *49* (21), 6177−6196.

(24) Amporndanai, K.; Meng, X.; Shang, W.; Jin, Z.; Rogers, M.; Zhao, Y.; Rao, Z.; Liu, Z. J.; Yang, H.; Zhang, L.; O'Neill, P. M.; Samar Hasnain, S. Inhibition mechanism of SARS-CoV-2 main protease by ebselen and its derivatives. *Nat. Commun.* **2021**, *12* (1), 3061.

(25) Muramatsu, T.; Takemoto, C.; Kim, Y. T.; Wang, H.; Nishii, W.; Terada, T.; Shirouzu, M.; Yokoyama, S. SARS-CoV 3CL protease cleaves its C-terminal autoprocessing site by novel subsite cooperativity. *Proc. Natl. Acad. Sci. U. S. A.* **2016**, *113* (46), 12997−13002.

(26) Sarma, B. K.; Mugesh, G. Antioxidant activity of the anti-inflammatory compound ebselen: a reversible cyclization pathway via selenenic and seleninic acid intermediates. *Chem. - Eur. J.* **2008**, *14* (34), 10603−10614.

(27) Haenen, G. R.; De Rooij, B. M.; Vermeulen, N. P.; Bast, A. Mechanism of the reaction of ebselen with endogenous thiols: Dihydrolipoate is a better cofactor than glutathione in the peroxidase activity of ebselen. *Mol. Pharmacol.* **1990**, *37* (3), 412−422.

(28) Wagner, G.; Schuch, G.; Akerboom, T. P.; Sies, H. Transport of ebselen in plasma and its transfer to binding sites in the hepatocyte. *Biochem. Pharmacol.* **1994**, *48* (6), 1137−1144.

(29) Singh, N.; Halliday, A. C.; Thomas, J. M.; Kuznetsova, O. V.; Baldwin, R.; Woon, E. C.; Aley, P. K.; Antoniadou, I.; Sharp, T.; Vasudevan, S. R.; Churchill, G. C. A safe lithium mimetic for bipolar disorder. *Nat. Commun.* **2013**, *4*, 1332.

(30) Johnson, T. W.; Dress, K. R.; Edwards, M. Using the Golden Triangle to optimize clearance and oral absorption. *Bioorg. Med. Chem. Lett.* **2009**, *19* (19), 5560−5564.

(31) Johnson, T. W.; Gallego, R. A.; Edwards, M. P. Lipophilic Efficiency as an Important Metric in Drug Design. *J. Med. Chem.* **2018**, *61* (15), 6401−6420.

(32) Hopkins, A. L.; Keseru, G. M.; Leeson, P. D.; Rees, D. C.; Reynolds, C. H. The role of ligand efficiency metrics in drug discovery. *Nat. Rev. Drug Discovery* **2014**, *13* (2), 105−121.

(33) Raymer, B.; Bhattacharya, S. K. Lead-like Drugs: A Perspective. *J. Med. Chem.* **2018**, *61* (23), 10375−10384.

(34) Weiss, M. M.; Dineen, T. A.; Marx, I. E.; Altmann, S.; Boezio, A.; Bregman, H.; Chu-Moyer, M.; DiMauro, E. F.; Feric Bojic, E.; Foti, R. S.; Gao, H.; Graceffa, R.; Gunaydin, H.; Guzman-Perez, A.; Huang, H.; Huang, L.; Jarosh, M.; Kornecook, T.; Kreiman, C. R.; Ligutti, J.; La, D. S.; Lin, M. J.; Liu, D.; Moyer, B. D.; Nguyen, H. N.; Peterson, E. A.; Rose, P. E.; Taborn, K.; Youngblood, B. D.; Yu, V.; Fremeau, R. T., Jr. Sulfonamides as Selective NaV1.7 Inhibitors: Optimizing Potency and Pharmacokinetics While Mitigating Metabolic Liabilities. *J. Med. Chem.* **2017**, *60* (14), 5969−5989.

(35) Dittmar, M.; Lee, J. S.; Whig, K.; Segrist, E.; Li, M.; Kamalia, B.; Castellana, L.; Ayyanathan, K.; Cardenas-Diaz, F. L.; Morrisey, E. E.; Truitt, R.; Yang, W.; Jurado, K.; Samby, K.; Ramage, H.; Schultz, D. C.; Cherry, S. Drug repurposing screens reveal cell-type-specific entry pathways and FDA-approved drugs active against SARS-Cov-2. *Cell Rep.* **2021**, *35* (1), 108959.

(36) Jang, W. D.; Jeon, S.; Kim, S.; Lee, S. Y. Drugs repurposed for COVID-19 by virtual screening of 6,218 drugs and cell-based assay. *Proc. Natl. Acad. Sci. U. S. A.* **2021**, *118* (30), No. e2024302118.

(37) Choi, S. W.; Shin, J. S.; Park, S. J.; Jung, E.; Park, Y. G.; Lee, J.; Kim, S. J.; Park, H. J.; Lee, J. H.; Park, S. M.; Moon, S. H.; Ban, K.; Go, Y. Y. Antiviral activity and safety of remdesivir against SARS-CoV-2 infection in human pluripotent stem cell-derived cardiomyocytes. *Antiviral Res.* **2020**, *184*, 104955.

(38) Tiwari, S. K.; Wang, S.; Smith, D.; Carlin, A. F.; Rana, T. M. Revealing Tissue-Specific SARS-CoV-2 Infection and Host Responses using Human Stem Cell-Derived Lung and Cerebral Organoids. *Stem Cell Rep.* **2021**, *16* (3), 437−445.

(39) Li, N.; Hui, H.; Bray, B.; Gonzalez, G. M.; Zeller, M.; Anderson, K. G.; Knight, R.; Smith, D.; Wang, Y.; Carlin, A. F.; Rana, T. M. METTL3 regulates viral m6A RNA modification and host cell innate immune responses during SARS-CoV-2 infection. *Cell Rep.* **2021**, *35* (6), 109091.

(40) Wang, S.; Li, W.; Hui, H.; Tiwari, S. K.; Zhang, Q.; Croker, B. A.; Rawlings, S.; Smith, D.; Carlin, A. F.; Rana, T. M. Cholesterol 25-Hydroxylase inhibits SARS-CoV-2 and other coronaviruses by depleting membrane cholesterol. *EMBO J.* **2020**, *39* (21), No. e106057.

(41) Ma, C.; Hu, Y.; Townsend, J. A.; Lagarias, P. I.; Marty, M. T.; Kolocouris, A.; Wang, J. Ebselen, Disulfiram, Carmofur, PX-12, Tideglusib, and Shikonin Are Nonspecific Promiscuous SARS-CoV-2 Main Protease Inhibitors. *ACS Pharmacol Transl Sci.* **2020**, *3* (6), 1265−1277.

(42) Weglarz-Tomczak, E.; Tomczak, J. M.; Talma, M.; Burda-Grabowska, M.; Giurg, M.; Brul, S. Identification of ebselen and its analogues as potent covalent inhibitors of papain-like protease from SARS-CoV-2. *Sci. Rep.* **2021**, *11* (1), 3640.

(43) Freitas, B. T.; Durie, I. A.; Murray, J.; Longo, J. E.; Miller, H. C.; Crich, D.; Hogan, R. J.; Tripp, R. A.; Pegan, S. D. Characterization and Noncovalent Inhibition of the Deubiquitinase and deISGylase Activity of SARS-CoV-2 Papain-Like Protease. *ACS Infect. Dis.* **2020**, *6* (8), 2099−2109.

(44) Shin, D.; Mukherjee, R.; Grewe, D.; Bojkova, D.; Baek, K.; Bhattacharya, A.; Schulz, L.; Widera, M.; Mehdipour, A. R.; Tascher, G.; Geurink, P. P.; Wilhelm, A.; van der Heden van Noort, G. J.; Ovaa, H.; Muller, S.; Knobeloch, K. P.; Rajalingam, K.; Schulman, B. A.; Cinatl, J.; Hummer, G.; Ciesek, S.; Dikic, I. Papain-like protease regulates SARS-CoV-2 viral spread and innate immunity. *Nature* **2020**, *587* (7835), 657−662.

(45) Klemm, T.; Ebert, G.; Calleja, D. J; Allison, C. C; Richardson, L. W; Bernardini, J. P; Lu, B. G.; Kuchel, N. W; Grohmann, C.; Shibata, Y.; Gan, Z. Y.; Cooney, J. P; Doerflinger, M.; Au, A. E; Blackmore, T. R; Heden van Noort, G. J; Geurink, P. P; Ovaa, H.; Newman, J.; Riboldi-Tunnicliffe, A.; Czabotar, P. E; Mitchell, J. P; Feltham, R.; Lechtenberg, B. C; Lowes, K. N; Dewson, G.; Pellegrini, M.; Lessene, G.; Komander, D. Mechanism and inhibition of the papain-like protease, PLpro, of SARS-CoV-2. *EMBO J.* **2020**, *39* (18), No. e106275.

(46) Liu, G.; Lee, J.-H.; Parker, Z. M.; Acharya, D.; Chiang, J. J.; van Gent, M.; Riedl, W.; Davis-Gardner, M. E.; Wies, E.; Chiang, C.; Gack, M. U. ISG15-dependent activation of the sensor MDA5 is antagonized by the SARS-CoV-2 papain-like protease to evade host innate immunity. *Nature Microbiology* **2021**, *6*, 467−478.

(47) Jacobson, M. P.; Friesner, R. A.; Xiang, Z.; Honig, B. On the role of the crystal environment in determining protein side-chain conformations. *J. Mol. Biol.* **2002**, *320* (3), 597−608.

(48) Jacobson, M. P.; Pincus, D. L.; Rapp, C. S.; Day, T. J.; Honig, B.; Shaw, D. E.; Friesner, R. A. A hierarchical approach to all-atom protein loop prediction. *Proteins: Struct., Funct., Genet.* **2004**, *55* (2), 351−367.

(49) Donovan, S. F.; Pescatore, M. C. Method for measuring the logarithm of the octanol-water partition coefficient by using short octadecyl-poly(vinyl alcohol) high-performance liquid chromatography columns. *J. Chromatogr A* **2002**, *952* (1−2), 47−61.

(50) Box, K.; Bevan, C.; Comer, J.; Hill, A.; Allen, R.; Reynolds, D. High-throughput measurement of pKa values in a mixed-buffer linear pH gradient system. *Anal. Chem.* **2003**, *75* (4), 883−892.